PET-RAFT COPOLYMERIZATION OF ISOCYANIDES AND VINYL MONOMERS TO ACCESS NOVEL POLYMERS

A Thesis

Presented to the Faculty of the Graduate School

of Cornell University

In Partial Fulfillment of the Requirements for the Degree of

Master of the Science of Chemistry

by

Cassandra Ann Haynes

August 2023

ABSTRACT

Due to the impending global plastic crisis, new polymerization strategies are needed to design degradable polymers which would render commercial polymers degradable via chemical hydrolysis, enzymatically, or photolytically. Of immense interest are carbonyl-containing polymers which are known to photodegrade under ultraviolet light. This would not only allow for the commercial materials with carbonyl incorporations to be chemically recycled but allow for plastic materials to degrade under environmental conditions if mismanaged.

The following thesis will entail how I employed photoinduced electron transfer – reversible addition fragmentation chain transfer (PET-RAFT) to copolymerize monomers with isocyanides to access novel, photodegradable copolymers. I was able to obtain three different novel copolymers, poly(MA-*co*-TosMIC), poly(MA-*co*-MEI), and poly(VAc-*co*-MEI), using this controlled radical polymerization method. I was able to tune the incorporation of the isocyanide within the backbone. Given the reactivity differences in each of these comonomer systems, I optimized each pair for molecular weight and incorporation control.

I conclude with post-polymerization modifications where I provide evidence that hydrolysis of the isocyanide can be leveraged to access the carbonyl along the polymer backbone. I propose future directions including post-polymerization functionalize with amines and crosslinking with diamines to access unique and potentially recyclable materials.

BIOGRAPHICAL SKETCH

Cassandra Haynes graduated from Lycoming College, Williamsport, PA in 2018 with a Bachelor of Science degree in chemistry and a minor in biology. Upon graduation, she started working for Corning Incorporated, Corning, NY, in the Organic and Biochemical Technologies research division. She began Cornell's Chemistry and Chemical Biology master's program in 2021.

ACKNOWLEDGMENTS

First off, I would like to thank everyone in the Stache lab for being kind and welcoming as I began my master's research. Not only were you all wonderful lab mates, but all you were inspiring scientists to work with and I am excited to see where your future endeavors lead each of you. To Erin, your career thus far has been incredibly inspirational. I am exceptionally thankful that I had the opportunity to learn from such an amazing scientist, teacher, and mentor.

I would like to thank Corning Incorporated for its support in allowing me to pursue my academic interests, I am incredibly thankful for being allowed this opportunity. Specifically, I would like to gratefully acknowledge Charles Brandenburg for his mentorship and for empowering me to pursue my career goals. I would like to thank Jenny Kim for encouraging me to grow my interests within this field through research opportunities at Corning. To Edward Fewkes, I would like to thank him for fueling my intellectual curiosity in the field of polymer and materials chemistry. Finally, I wish to thank all my supportive coworkers within the Organic and Biochemical Technologies group, you have helped make this pursuit enjoyable and are such wonderful group to work with.

Finally, I would like to give thanks to all my family and friends that have cheered me on through this endeavor. Especially to my mom, dad, and sister for always encouraging me to reach for the stars. Last, but not least, I would like to thank my husband, Dylan, for standing by me and being incredibly supportive as I worked towards this milestone.

TABLE OF CONTENTS

LIST OF FIGURES

LIST OF TABLES

LIST OF SCHEMES

1.1 Introduction

1.1.1 Background on the plastic crisis and recycling alternatives

Plastics have saturated our society since mass production began in the 1940s, and alarmingly, every piece of plastic produced still exists today in some shape or form, whether still in use, disposed of, or incinerated to a gaseous waste product.[1] Our society has deemed plastics a "workhorse material", coming in a variety of different forms and colors while providing access to functional application, durability, low toxicity, and a high strength-to-weight ratio, all while being inexpensive to manufacture.[2] This ubiquitous material is termed "plastic" due to its ability to be formed and molded by applied heat and pressure. Plastic materials are made up of polymers, which are large chains of molecules consisting of repeating smaller units. These small repeating units known as monomers are polymerized into a polymer chain through a variety of methods. Most monomers are obtained through refinement of fossil fuels, an unrenewable resource, which is rapidly being depleted.

Alarmingly, the OECD Global Plastics Outlook Database states plastic production hit 460 million tonnes (Mt) in 2019, increasing by twenty-fold over the past fifty years.[3] Production is expected to double over the next twenty years due to the ever-growing demand, which is a major cause for concern due to the dwindling and controversial supply of the unrenewable starting material. Additionally, plastics are typically one-time use, giving a product an undesirable turn-over time with two-thirds of waste generated being less than five years old.[3] With the global recycling rate only being 9%, the current lifecycle of a plastic is linear with no effective way to regenerate the starting material. Majority of the waste is disposed in a landfill (49%), incinerated (19%), or mismanaged (23%).[3] The mismanaged materials either end up in uncontrolled dumpsites, burned in unauthorized pits, or dumped into aquatic waterways.[3]

A significant portion of landfills are filled with one-time use plastic materials including plastic bags, bottles, and packaging products. The incineration of plastic waste adds to the harmful greenhouse gas emissions, and littered plastics that enter the aquatic waterways are detrimental to the ocean life via ingestion, entanglement, and/or smothering.[2,3] If actions aren't taken soon, by weight, there will be more plastic waste in the ocean than fish by 2050.[4] Current plastic materials additionally contain stabilizers, plasticizers, and pigments, which are additives used to increase a plastic's half-life. Not only does this ensure plastics will be around longer if mismanaged, but evidence supports that under the right conditions the harmful additives can be released over time, enabling polymer decay to macro/microplastics, potentially causing further harm to our ecosystem.[2,4]

The inherent convenience of plastic material production and use is disproportioned to the disposal and recycling methods currently in place. This raises serious concern and potential crisis if alternative solutions are not implemented. There is a need to optimize how the global economy produces, reuses, and recycles plastic materials with the current recycling rate being only 9%.[4] Additionally, current recycling methodologies are unsustainable. Mechanical grinding and heating typically degrades the original desirable properties, yielding reuse in lower value applications, which aren't eligible to be recycled a second time.[4] The Ellen MacArthur Foundation advocates and researches circular economy benefits that will impact global challenges. They have proposed a promising circular economy approach to optimize the stages in a plastic's lifecycle. This avenue would feature chemical recycling of plastics and mixed plastics back to monomeric or oligomeric units, which would avoid the loss in value inherent in methods using mechanical recycling.[4]

1.1.2 Chemistry to access photodegradable polymers

In response to the impending global crisis, researchers have been working to develop new

chemistries to access degradable polymers. By accommodating chemical recycling, synthetic design can be employed to add reactive main chain functional groups that can be hydrolyzed chemically, enzymatically, or otherwise cleaved to yield oligomers or monomeric units.[5] Commercial plastics, such as polyethylene and polystyrene, are inert polymers with all-carbon backbones.[5] Design of degradable polymers containing carbon-oxygen bonds is of immense interest because at low incorporation levels, the ubiquitous properties of a polymer are maintained, and the in-chain carbon-oxygen bonds can absorb specific light radiation to initiate photodegradation.[6]

Specifically, global researchers are interested in the addition of carbonyl moieties. At low incorporations, commercial materials can be photodegraded back to monomeric and oligomeric components via Norrish cleavage reactions, accessing a chemical recycling avenue. Norrish Type I reactions lead to alpha bond cleavage forming an acyl and alkyl radical, but more interestingly (Figure 1), Norrish Type II reactions lead to intramolecular gamma hydrogen abstraction by an excited carbonyl group to produce a 1,4-diradical species (Figure 2).[6] This 1,4-diradical species can cause bond scission between the alpha and beta carbon to produce an enol and an olefin.[6] This reaction potentially provides a unique pathway to chemically recycle polymers with low carbonyl incorporations back to olefin monomer.

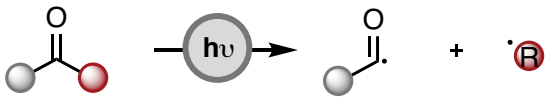

Figure 1: Norrish Type I reaction

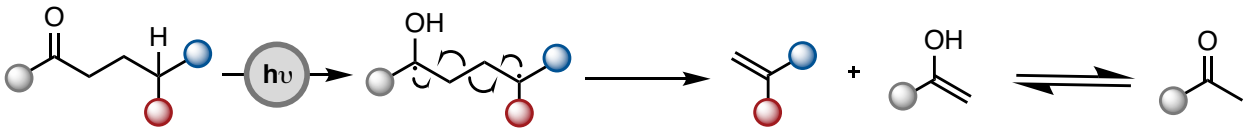

Figure 2: Norrish Type II reaction

1.1.3 Existing chemical approaches to access in-chain carbonyls

Historical methods to insert carbonyls within polymers involve the copolymerization of ethylene and carbon monoxide. Farbenfabriken Bayer first reported and patented the free radical copolymerization of these comonomers in 1941. Using harsh reaction conditions with high temperatures and pressures, they were able to obtain polymers termed polyketones.[7] Almost ten years later, Reppe and Brubaker at Dupont (1950) implemented a nickel (II) catalyst while keeping reaction conditions at the comparatively more gentle conditions of 200 °C and 400 atm, so as to obtain the polymerization of polyketones.[7] These methods obtained low molecular weight polymers that exhibited serious drawbacks including crosslinking, high viscosity, and high melt temperatures.[7,8] Due to the poor physical properties, these polyketones could not be commercialized, but modifications to the synthesis process followed in the next few decades to afford both alternating and random polyketones.[7]

Drent at Shell made a real breakthrough in polyketone synthesis in 1983. Through the modification of a palladium (II)-based catalyst with a diphosphine ligand and weakly coordinating anions, higher molecular weight polyketones were accessed at relatively mild reaction conditions, 90 °C and ~ 50 atm.[9] Access to more desirable melt properties were also achieved with the addition of propene, higher aliphatic α-olefins, functionalized α-olefins, styrene, and 1,2-dienes.[9]

Continued catalyst development continued at Shell led by scientists, Nozaki, Hart, and Drent. Through modifications of a di-cationic palladium (II) complex, they took advantage of carbon monoxide's higher affinity for the palladium's metal center and used coordination-insertion

chemistry to afford perfectly alternating polyketones.[10] The perfectly alternating ethene and carbon monoxide polymers provided access to a semi-crystalline thermoplastic that exhibited high temperature chemical and mechanical resistance, wear resistance, and desirable barrier properties. Shell Chemical commercialized this process in 1996 under the product name Carilon®.[9] The industrial product had potential to import these polymers in a broad range of engineering, barrier packaging, and material applications. Unfortunately, Shell discontinued the production in 2000 due to continued processing difficulties brought on by the limited solubility and high melt processing temperatures (Tm ~ 260 °C) of the perfectly alternating polyketone.[9] Drent persevered and implemented the first neutral palladium (II) catalyst to access the first non-alternating, linear polyketone that did not contain branching side chains found in the free radical polymerizations of ethene and carbon monoxide.[9]

Sen and Muller recognized that introduction of lower amounts of carbonyls into the backbone accessed similar desirable properties found in homopolymers of ethene. Separately, they both published papers where they executed disproportionate feed ratios and coordination-insertion polymerizations to access 1.5 mol% incorporation of carbon monoxide with ethylene.[11,12] However, undesirable carbonyl clustering was observed with this method. This is unfavorable when considering degradation pathways because the carbonyls should be randomly spaced throughout the backbone of a polymer to get optimal degradation to oligomeric and monomeric units.[11,12]

More recent work in 2016, completed by Arrington and coworkers, involved designing cyclic monomers for ring-opening metathesis polymerization. They were able to achieve both regular and irregular spacing of in-chain ketones through this design. The ketones were spaced every six methylene units apart and exhibited lower melting ranges (160-165 °C) than alternating

polyketones from ethylene and carbon monoxide.[13] In 2020, Mecking and co-workers were able to synthesize low density polyethylene with in-chain ketone groups at low incorporation levels through modifications of solvent, pressure, and temperature. They studied the reactivity ratios of ethylene and carbon monoxide as well as the physical properties of the lower incorporated copolymers. The group was able to observe polymer degradation via chain scission by Norrish Type I and Type II reactions, while gaining valuable insight in the reactivity of the acyl radical generated post carbon monoxide insertion.[14]

Additionally, more investigations have been taking place to improve the coordination-insertion polymerization method. In 2021, Chen and coworkers published their research which studied the use of cationic palladium complexes with ligand modifications. By installing strong electron-donating groups on the ligated species, the palladium center became highly active allowing for efficient non-alternating copolymerization of ethylene and carbon monoxide monomers.[15] Later that same year, Nozaki and coworkers employed metal carbonyls as an alternative to toxic carbon monoxide gas and were successfully able to synthesize non-alternating, linear ethylene/carbonyl copolymers with very low carbonyl content. This high-density polyethylene (HDPE) similar material retained the desirable physical properties of commercial HDPE but was also found to be photodegradable when treated with UV light.[16]

Continuing to establish an understanding of the mechanism of chain growth when reacting ethylene and carbon monoxide comonomers, the 2022 work pioneered by Mecking and coworkers looked at the mechanistic difference with Ni(II) phosphinephenolate catalysts versus traditional Pd(II) phosphinesulfonate complexes to afford the desirable random non-alternating polyketones through exploration of differences with their rate-determining steps.[17] Through steric hinderance and electron donation, Mecking was able to employ modifications to the ligands on the Ni(II)

phosphinephenolate catalyst to increase favorability of the desired non-alternating pathway when copolymerizing carbon monoxide with ethylene.[17]

1.1.4 A novel, alternative avenue to access in-chain carbonyls

Most recently, work done by the Stache group employed a cobalt-mediated radical polymerization (CMRP) with cobalt-hydride (Co-H) as a discrete and rapid initiator to copolymerize acrylate monomers with an isocyanide (Scheme 1).[18,19] This is an attractive approach in comparison to the radical copolymerizations with carbon monoxide because it avoids the use of the toxic and odorless gas while preventing the rapid decarbonylation reaction that occurs with activated monomers unless under exceedingly high pressures.[15] The typical ethylene and carbon monoxide copolymer also has a competitive pathway where the propagating chain's reactive acyl radical can intramolecularly abstract a hydrogen causing chain transfer and branching events.[16] Isocyanides are ambiguously like carbon monoxide because they present the same isoelectronic properties, and they are easier to handle while providing the opportunity to tune the electronics of the desired isocyanide.[18]

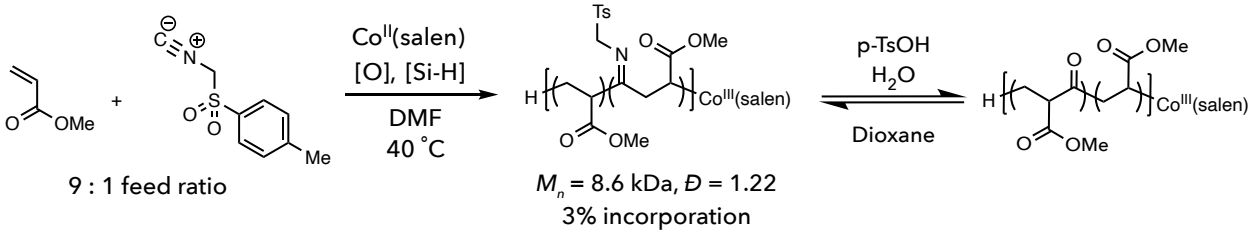

Scheme 1: Discrete Co-H initiated CMRP to obtain poly(MA-*co*-TosMIC) then hydrolysis to afford poly(MA-*co*-ketone)

Stache's work proved that the isocyanide can undergo radical addition like carbon monoxide while also providing control over the stoichiometry and slower *a*-scission rates.[18] However, the reactive imidoyl radical formed can undergo competitive β-scission to form nitriles or hydrogen atom abstraction like the acyl radical.[18] By implementing the reversible deactivation

radical polymerization (RDRP) method though, they were able to control the radical concentration, which reduced the unproductive termination and chain transfer events allowing for control over molecular weight, dispersity, and incorporation of isocyanides to access a novel poly(acrylate-*co*-isocyanide) copolymer.[18] The isocyanide moiety was then susceptible to hydrolysis affording the desired carbonyl which was then shown to photodegrade via Norrish cleavage under UV light.[18]

Poly(acrylate-*co*-isocyanide) obtained using the Co-H CMRP protocol was very successful for acrylate monomers. However, expanding the approach to other classes of monomers and copolymers continued to be investigated, as Co-H initiation was ineffective for less-activated monomers. Several other RDRP methods exist, and employing alternative protocols would allow access to different initiation methods and alternative monomers and isocyanide combinations. In the following thesis, I will detail how photoinduced electron transfer - reversible addition fragmentation chain transfer (PET-RAFT) polymerization was employed to obtain novel copolymers with a broadened monomer and isocyanide scope as well as conditions for post polymerization modifications.

2.1 PET-RAFT to obtain poly(acrylate-*co*-isocyanide)

2.1.1 Introduction to PET-RAFT

PET-RAFT was envisioned as an alternative RDRP method to Co-H CMRP due to the prospect of initiating the polymerization with light instead of heat, as well as leveraging this method to access a broader monomer scope. The discrete Co-H initiated CMRP conditions do not initiate vinyl acetate (VAc) polymerization, and this was one of monomers I wished to add to the copolymer scope.[19] As an appealing alternative, reversible addition fragmentation chain transfer (RAFT) polymerizations are versatile and present the ability to obtain predictable molecular weights with low dispersities while providing chain "livingness".[20] A key feature of RAFT is the chain transfer agent (CTA), which enables the RAFT equilibrium between active propagating radical species and dormant polymer chains capped with the CTA. By modifying the CTA, targeted molecular weight distributions can be achieved by tuning the rate of addition/fragmentation with the CTA. Polymers prepared via RAFT can be further extended by reactivating the CTA and adding more monomer.[20]

Traditional RAFT polymerizations are thermally initiated; however, in 2014 the Boyer group was able to modify this process and initiate the RAFT process with light, terming this method photoinduced electron transfer (PET) – RAFT.[21] Through light excitation of a photocatalyst, a RAFT agent can be reduced to initiate a radical polymerization while also acting as the chain transfer agent to control the polymerization growth through the RAFT equilibrium (Scheme 2).[21]

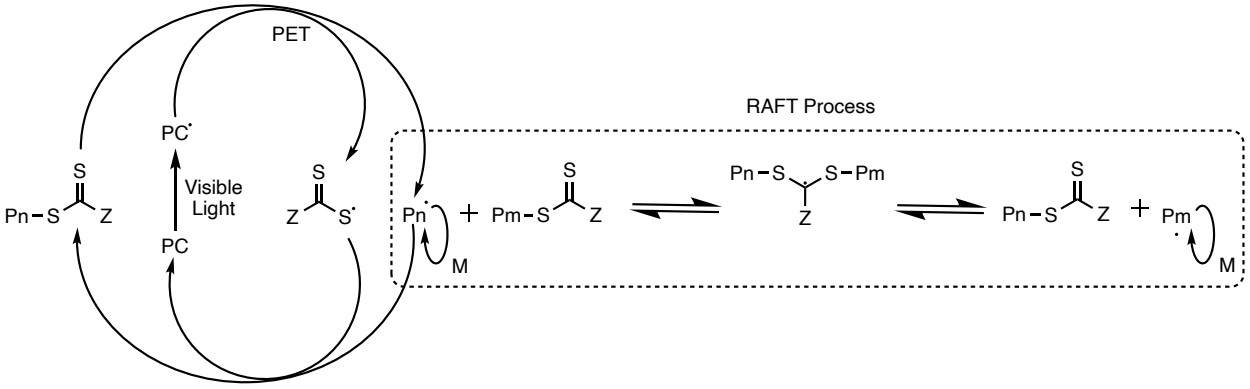

Scheme 2: General PET-RAFT mechanism

2.1.2 Obtaining poly(MA-*co*-TosMIC) via PET-RAFT

The Stache group's previously reported copolymerization of methyl acrylate (MA) (Scheme 3 - 1) and *p*-toluenesulfonylmethyl isocyanide (TosMIC) (Scheme 3 - 2) via the Co-H CMRP protocol was used as a control and baseline (Table 1 – entry 1). As a proof of concept, I employed free radical polymerization initiated by either benzoyl peroxide or azobisisobutyronitrile (AIBN) to afford the desired copolymer, however, the reaction was uncontrolled and presented high dispersities due to the free radical nature creating branching and chain scission events (Table 1 – entry 2).

I then evaluated the effectiveness of the PET-RAFT method to compare with the CMRP obtained poly(MA-*co*-TosMIC). Implementing the PET-RAFT protocol (Scheme 3), I targeted an incorporation of 3% TosMIC. I obtained copolymers with similar molecular weight and incorporation of TosMIC as observed with the Co-H CMRP protocol (Table 1 – entries 1 & 3). I also proved that higher degrees of polymerization (DPs) could be targeted to provide larger polymers while maintaining similar TosMIC incorporations seen with lower DPs while maintaining low dispersities (Table 1 – entries 4 & 5).

Table 1: Molecular weight, dispersity, and incorporation for poly(MA-*co*-TosMIC)

Entry	Deviation	DP	M_n, th (kg/mol)	M_n, pure (kg/mol)	$Đ$	Experimental Incorporation	Theoretical Incorporation
1[a]	Co-H CMRP	200	7.2	8.6	1.22	2.6%	5.6%
2	Free Radical	40	N/A	2.4	2.09	6.4%	9.2%
3		200	7.6	7.1	1.12	2.2%	4.8%
4		400	15.7	15.6	1.16	2.4%	3.3%
5		800	34.8	22.4	1.39	2.5%	2.9%

[a]Entry from reference 18

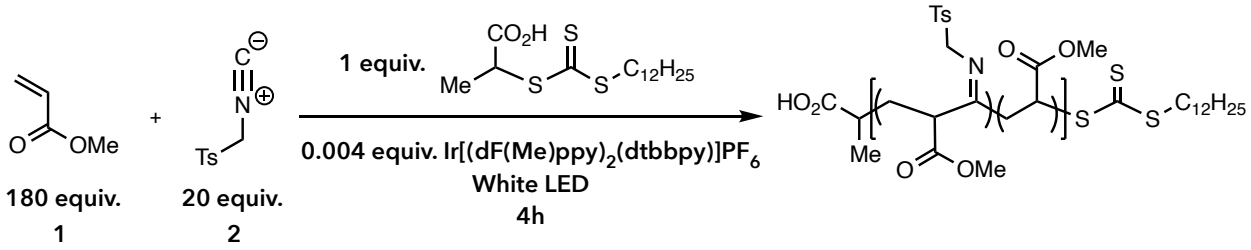

Scheme 3: Standard copolymerization conditions to obtain poly(MA-*co*-TosMIC)

2.1.3 Unique properties of incorporated TosMIC observed

To continue this copolymerization study, I wanted to ensure that the copolymers obtained via the PET-RAFT protocol exhibited similar conformational properties the Stache group observed with their isocyanide incorporated copolymers. Through extensive NMR characterization on poly(MA-*co*-TosMIC) the Stache group found that the β-imine ester is the kinetically favored product of the polymerization.[18] This was observed at the 4.7 ppm shift of the methylene protons of the 0 h ^{1}H NMR (Figure 3). As the sample was exposed to protic solvents, the copolymer thermodynamically tautomerized into the β-enamine ester, which was directly incorporated into the backbone of the polymer.[18] As this occurred the methylene protons became diastereotopic causing a broadening of the methylene peaks, evident in the 17 h ^{1}H NMR (Figure 3).[18] Another β-enamine ester peak was also observed downfield at 9.4 ppm and corresponded to the enamine proton post tautomerization.[18]

I expected and did observe the same conformational change within the PET-RAFT

obtained poly(MA-*co*-TosMIC) copolymers. The tautomerization to the enamine was preferred thanks to the stability established within a pseudo six-membered, hydrogen-bonded ring.[18] Observation of this tautomer within this system was exciting because we could imagine accessing multiple conformations and additional in-chain transformations.

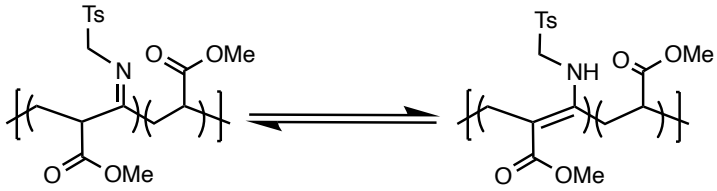

Scheme 4: Tautomerization from imine to enamine

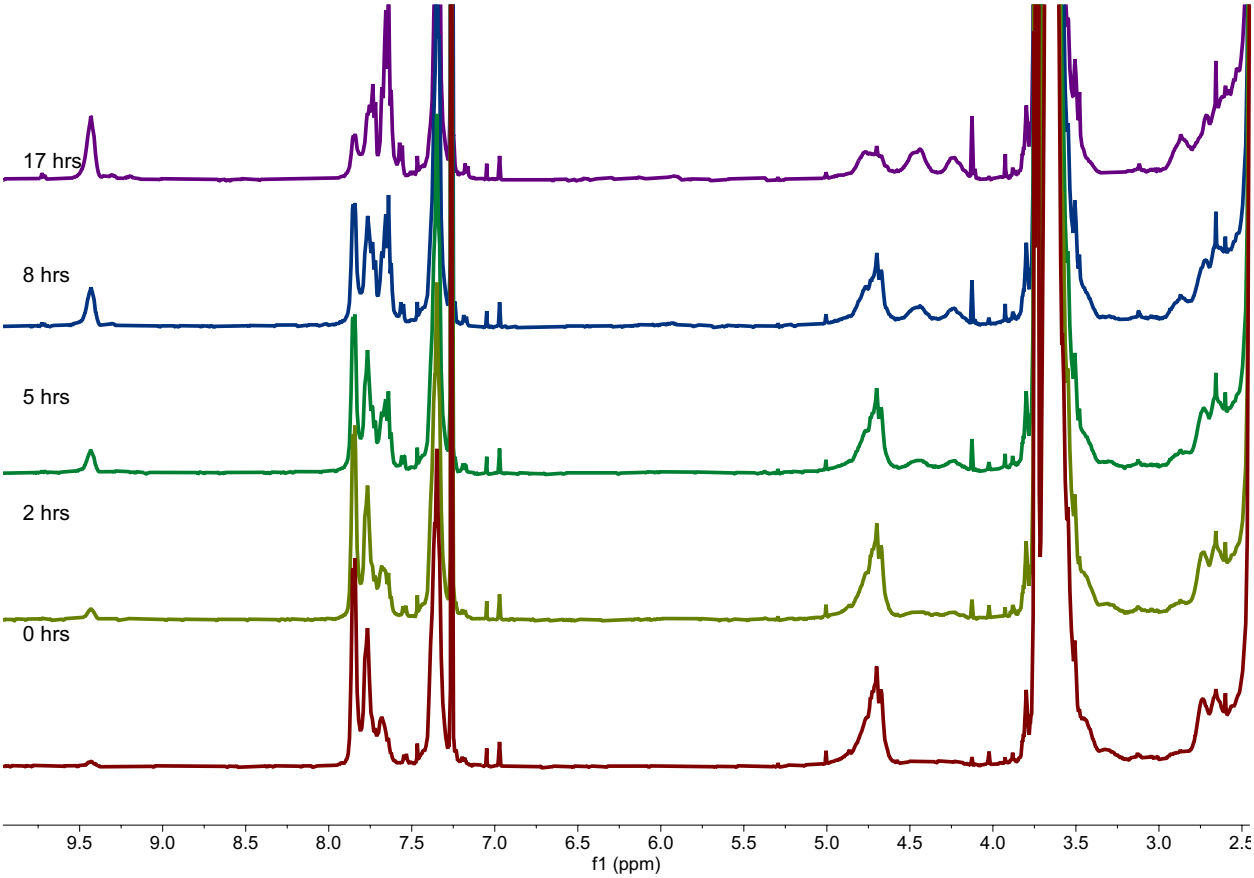

Figure 3: ^{1}H NMR timed study of the tautomerization of poly(MA-*co*-TosMIC) obtained from Camdzic, L. Stache, E. E. "Controlled radical polymerizations of acrylates and isocyanides installs degradable functionality into novel copolymers – supporting information," *in revisions.*

Another evident conformational change I observed within the copolymers obtained via

PET-RAFT was the formation of a lactam within the backbone of the copolymer post tautomerization to the β-enamine ester. The Stache lab also observed the same lactam formation with the Co-H CMRP copolymers, although only at low amounts and evident with a proton at a shift of 9.2 ppm of a ^{1}H NMR.

Although further characterization will need to be done, the proposed mechanism is below in Scheme 5. The nucleophilic enamine's lone pair of electrons attacks the π* orbitals of the ester's carbonyl carbon delocalizing the electrons to the oxygen. Then the carbonyl is reformed, and methoxide is released, and further acts as a strong base to deprotonate the amine. Next, the lone pair of electrons collapse, causing the tosyl group to leave and an iminium to form. This species is known to have a very short lifespan because any amount of acid present will react with the iminium to release formaldehyde and protonate the nitrogen again, producing the lactam along the backbone of the polymer.

Accessing the lactam has the potential to increase the glass transition temperature of the copolymers and introduce rigidity, which could lead to interesting physical properties. Future studies will potentially focus on reaction conditions to favor the equilibrium towards this conformation.

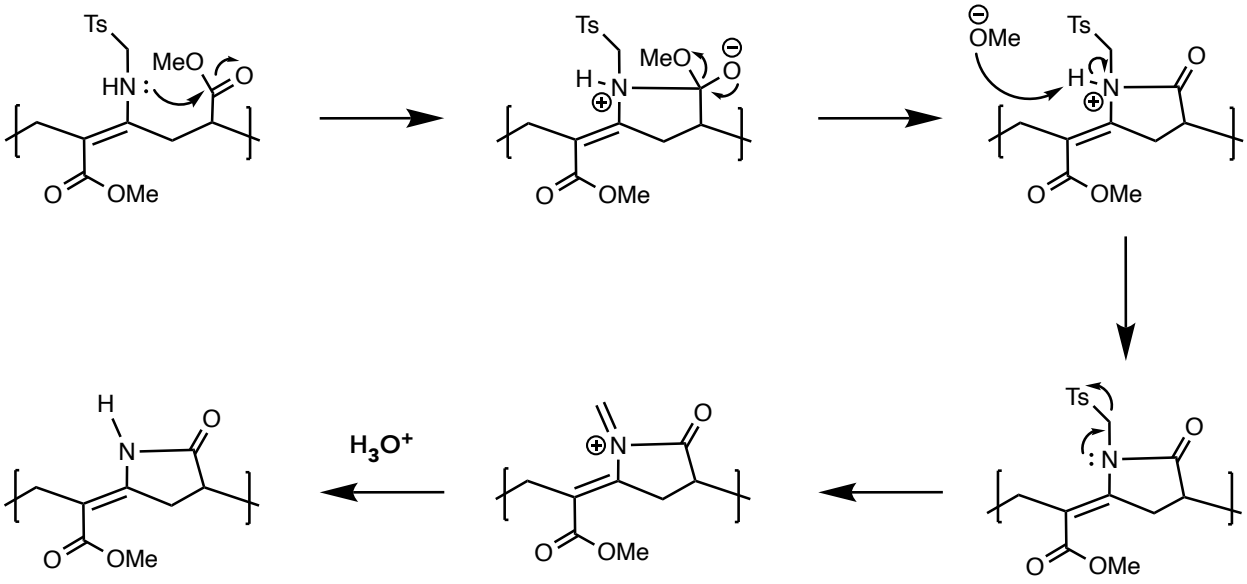

Scheme 5: Proposed cyclization mechanism to form lactam

2.1.4 Feed ratio modifications to tune TosMIC incorporation

Next, it was imperative to ensure that I could apply the PET-RAFT protocol to obtain tunable incorporations of TosMIC as seen with the Co-H CMRP method. The Stache group modified the comonomer feed ratios to obtain poly(MA-*co*-TosMIC) ranging from 3% to 35% TosMIC incorporation. To accomplish this with the PET-RAFT protocol, I also modified the feed ratios and was able to obtain copolymers that ranged from 2.2% to 7.7% incorporation of TosMIC (Table 2).

Comparatively to the Co-H CMRP protocol, as higher incorporations of TosMIC were targeted, the dispersity of the copolymer increased. This was indicative to loss of control over the propagation of monomers or is potentially due to the steric bulk of the TosMIC along the backbone. As the incorporation of the isocyanide increased, the polymer chains potentially moved through the GPC polystyrene standardized column differently than they would at lower incorporations. Also, the amount of isocyanide incorporated was lower than the theoretical percentage calculated. I expected this based on the differences seen using the Co-H CMRP protocol and it may be due to

potential side reactions not fully understood yet.

Table 2: Tunable incorporations of TosMIC, controlled molecular weight, and dispersities via PET-RAFT

Feed Ratio	M/I % conv.	M_n, crude (kg/mol)	$Đ$	M_n, theo. (kg/mol)	% incorp.	Theo. % incorp.
180:20	52/17	5.0	1.36	9.1	2.2%	3.5%
160:40	41/15	3.7	1.35	7.2	4.7%	8.4%
140:60	29/13	2.3	1.41	5.4	7.7%	16.1%

With the Co-H CMRP protocol, the Stache group reported kinetic and reactivity ratio studies. They found that as more MA was consumed, there was no evidence of an increase in TosMIC consumption, which indicated that TosMIC did not homopropagate and minimal compositional drift was observed. Also, they observed slower rates of polymerization as the amount of isocyanide present was increased in the system relative to the propagating chains. This helped affirm the copolymer microstructure stayed consistent with random incorporations of TosMIC along the backbone.

I was able to replicate the study using the PET-RAFT protocol to confirm similar behavior. I targeted 5% TosMIC incorporation and obtained a linear, first order plot for the consumption of MA and TosMIC (Figure 4). This helped solidify that the PET-RAFT protocol also could be implemented to access copolymers with tunable but random incorporations of TosMIC as desired.

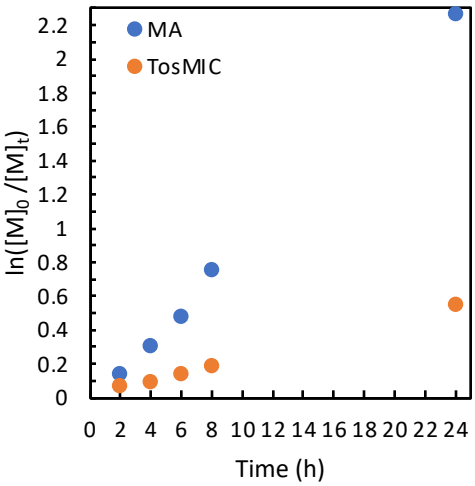

Figure 4: MA and TosMIC copolymerization kinetics

2.1.5 Scaling up poly(MA-*co*-TosMIC)

Unique to my research, I wanted to provide evidence that the PET-RAFT protocol could be applied to obtain the copolymers at a larger scale. Whereas the Co-H CMRP protocol employed heat to obtain the isocyanide incorporated copolymers, applying light to aid in the initiation of the polymerization would potentially allow us to produce these copolymers within a flow reactor at the industrial scale.

To begin this study, conditions to scale up the production of poly(MA-*co*-TosMIC) via PET-RAFT were established (Scheme 3) and a range of comonomer concentrations were targeted for a batch reaction. Within four hours, the larger-scale polymerizations produced similar molecular weights to the theoretically calculated molecular weights with low dispersities and targeted incorporations of TosMIC (Table 3). These results were exciting, and allowed us to continue this research by employing the protocol within a small scale flow reactor.[22]

Table 3: Scale-up data of poly(MA-*co*-TosMIC)

Entry	Scale	M_n, th (kg/mol)	M_n, pure (kg/mol)	$Đ$	Experimental Incorporation
1	4 mmol	7.6	7.1	1.12	2.2%
2	20 mmol	9.7	8.5	1.18	2.3%
3	100 mmol	5.5	5.2	1.16	3.3%

I was able to set-up the flow reactor and establish the necessary conditions to obtain the desired poly(MA-*co*-TosMIC) copolymer (Scheme 6). I used the flow reactor set-up to target 5% incorporations of TosMIC. Unfortunately, preliminary results at the five and twenty-five mmol scale showed small copolymers with low incorporations of TosMIC, but this was a promising starting point for future work where a flow reactor could be used to obtain the copolymer via this vital industrial scale up procedure (Table 4).

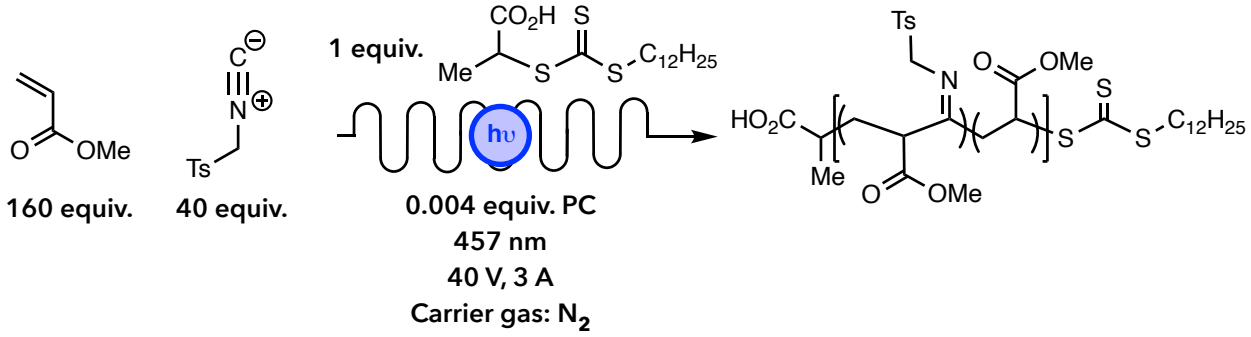

Scheme 6: Conditions for flow reactor set-up

Table 4: Flow reactor data of poly(MA-*co*-TosMIC)

Entry	Scale	Flow Rate (mL/min)	M_n, th (kg/mol)	M_n, crude (kg/mol)	$Đ$	Experimental Incorporation
1	5 mmol	1.0	5.3	2.1	1.34	3.2%
2	25 mmol	1.0	3.9	1.6	1.34	3.9%

3.1 Expanded isocyanide scope to include 2-morpholinoethyl isocyanide

3.1.1 Interest in isocyanide alternatives and initial reaction design

I hoped to expand the scope of the copolymerizations between monomers and isocyanides by selecting an electronic and steric alternative isocyanide to compare with TosMIC. 2-morpholinoethyl isocyanide (MEI) (3) piqued our interest and was chosen for the subsequent copolymerizations. TosMIC's tosyl group is electron withdrawing and aromatic whereas MEI has a two-carbon alkyl chain, which could help avoid the undesired β-scission, as well as an appending cyclic morpholino group. I expected poly(MA-*co*-TosMIC) to possess different physical, structural, and thermal properties than poly(MA-*co*-MEI). These differences are important when targeting polymers for specific applications. To obtain poly(MA-*co*-MEI), I hypothesized that the standard conditions which had allowed us to obtain poly(MA-*co*-TosMIC) would work when introducing MEI for the copolymerization (Scheme 7).

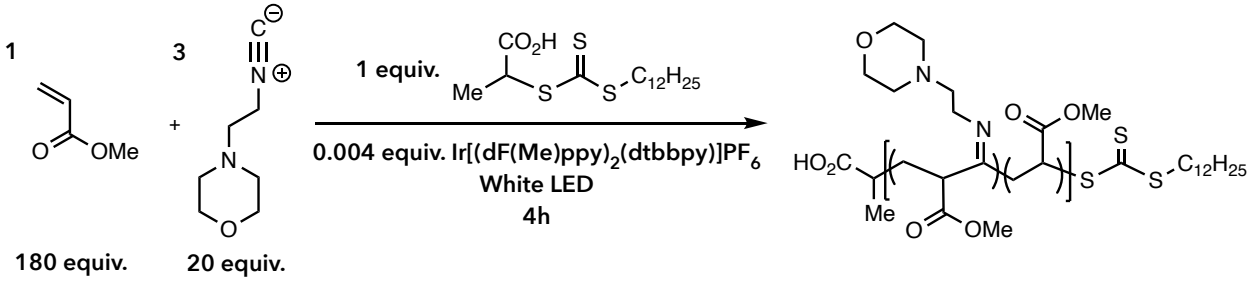

Scheme 7: Initial conditions to obtain poly(MA-*co*-MEI)

3.1.2 Tuning and determining the incorporation of MEI with the initial conditions

With the established protocol (Scheme 7), I targeted different feed ratios to tune the incorporation of MEI within the polymer as I had done previously with TosMIC. I made observations of ^{1}H NMR to determine which signals corresponded to the respective protons along the backbone of the copolymer. I expected to observe tautomerization to the β-enamine ester (9.4 ppm), as seen the with poly(MA-*co*-TosMIC), as well as proton signals indicating MEI

incorporation around 3.7 ppm, 3.5 ppm, 2.7 ppm, and 2.5 ppm. The highlighted areas showed an increase in intensity of the proton signals as higher incorporations of MEI were targeted (Figure 5). These were found as expected within shifts for incorporation of MEI. Also, the expected proton shift observed at 9.4 ppm indicated that the β-enamine ester was formed via tautomerization within this copolymer.

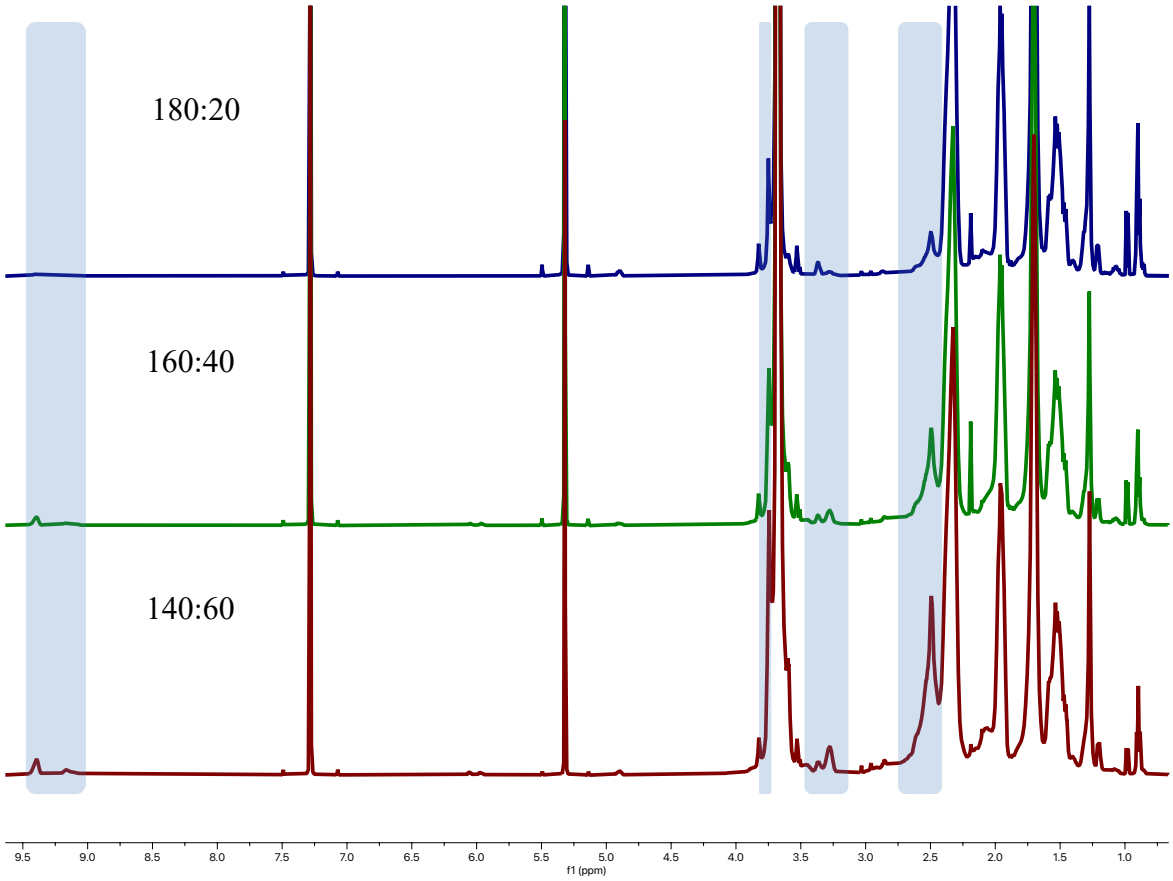

Figure 5: ^{1}H NMR provided evidence of increased MEI incorporation

Although proton signals increased in the expected areas, I was curious about integrated ratios I was observing with the spectra. The integrated ratio of the protons at the 2.5 ppm signal to the 3.7 ppm signal was 8:4. I had expected an even ratio of 6:6 protons to be observed. This prompted further investigation into the microstructure by using a prediction tool within the NMR MestReNova software to observe the imine to enamine tautomerization present within these

copolymers (Scheme 8 & Figure 6). The prediction tool suggested the methylene protons adjacent to the imine shifted from 2.6 ppm to 3.3 ppm after tautomerizing to the enamine (Figure 6). Therefore, I believed the ^{1}H NMR signals at 2.5 ppm and 3.3 ppm correspond to eight protons of an incorporated MEI moiety that has tautomerized to the thermodynamically favored conformer, and the four protons found around the morpholino's more electron withdrawing oxygen are downfield at 3.7 ppm. This rationalized the integrated 8:4 ratio I was obtaining.

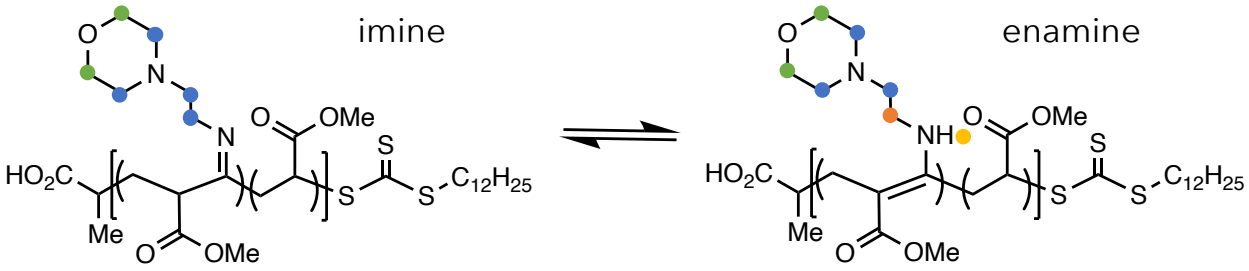

Scheme 8: Tautomerization observed with poly(MA-*co*-MEI)

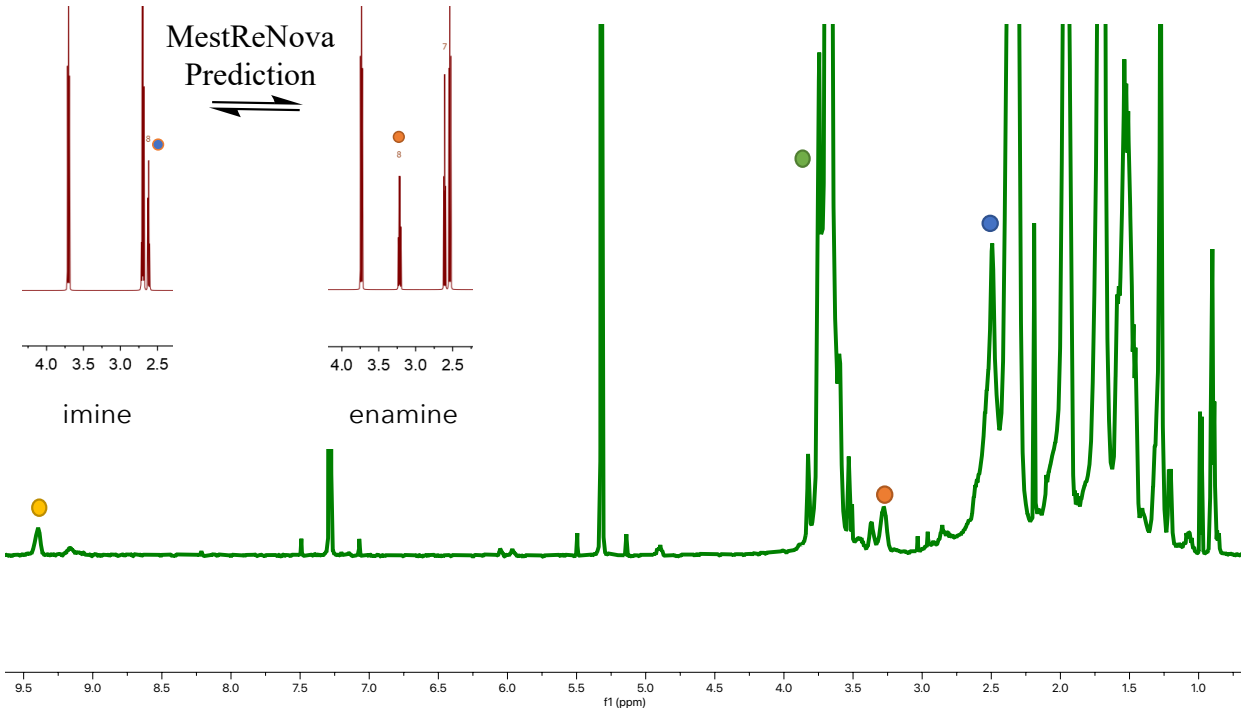

Figure 6: ^{1}H NMR evidence of tautomerization and MestReNova prediction software evidence of tautomerization

3.1.3 Calculating incorporation of isocyanides

After deducing the peaks which represented MEI incorporation, I needed to determine a method to calculate the percent of isocyanide incorporated into the backbone of the polymer. Regardless of polymerization method, Equation 1 represents how the incorporation of TosMIC was determined. Following this example and my new insight on the proton signals which corresponded to incorporated MEI, I formulated Equation 2. The ability to determine how much isocyanide was incorporated within the backbone of the copolymer was necessary to ensure we could tune and control the incorporation of MEI. Table 5 provides the incorporation data I calculated after deducing the structure via ^{1}H NMR.

$$\%\ TosMIC\ incorp. = \frac{(TosMIC\ methylene\ protons)}{(TosMIC\ methylene\ protons) + \left({}^{2}/_{3} * MA\ methoxy\ protons\right)}$$

Equation 1

$$\%\ MEI\ incorp. = \frac{\left({}^{3}/_{8} * MEI\ methylene\ protons\ adjacent\ to\ both\ nitrogens\ \right)}{(MA\ methoxy\ protons) + \left({}^{3}/_{8} * MEI\ methylene\ protons\ adjacent\ to\ both\ nitrogens\right)}$$

Equation 2

Table 5 – PET-RAFT data from poly(MA-*co*-MEI), high dispersities observed

Feed Ratio	M/I % conv.	M_n, pure (kg/mol)	$Đ$	M_n, theo. (kg/mol)	% incorp.	Theo. % incorp.
Free Radical	61/6.8	21.3	2.97	N/A	3.8%	2.7%
180:20	83/16	13.3	1.67	13.7	1.9%	2.1%
160:40	74/14	10.4	1.73	11.3	4.2%	4.5%
140:60	63/9.7	10.7	1.55	8.8	7.3%	6.2%

3.1.4 Troubleshooting with MEI

Although I was successfully able to calculate the incorporation of MEI within the copolymer backbone, the gel permeation chromatography (GPC) data presented polymers with

high dispersities. Implementing a controlled radical polymerization with the CTA should ideally produce copolymers with low dispersities less than 1.50, and this was one the goals I was hoping to accomplish with the copolymer.

To investigate why I was observing high dispersities I executed kinetic studies on the copolymerization between MA and MEI. I expected to observe similar kinetic behavior with this copolymerization as seen with poly(MA-*co*-TosMIC) and hoped that it would provide insight between copolymerizing with an alkyl versus an aromatic isocyanide. Surprisingly, the results obtained were not as expected (Figure 7). Monomer and isocyanide conversion was minimal over an eight hour period, unlike what I had observed with the poly(MA-*co*-TosMIC) system, which presented a steady linear upward trend (Figure 4). Additionally, ^{1}H NMR (Figure 8) showed no evidence of the CTA's omega-chain end in the expected locations of 3.37 ppm and 4.90 ppm. These perplexing results led to further investigation into the reaction components.

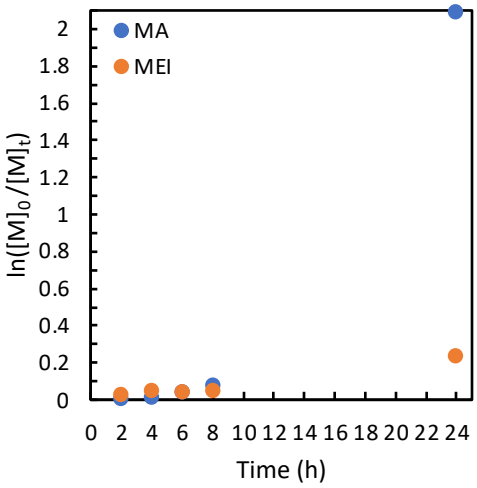

Figure 7: MA and MEI copolymerization kinetics

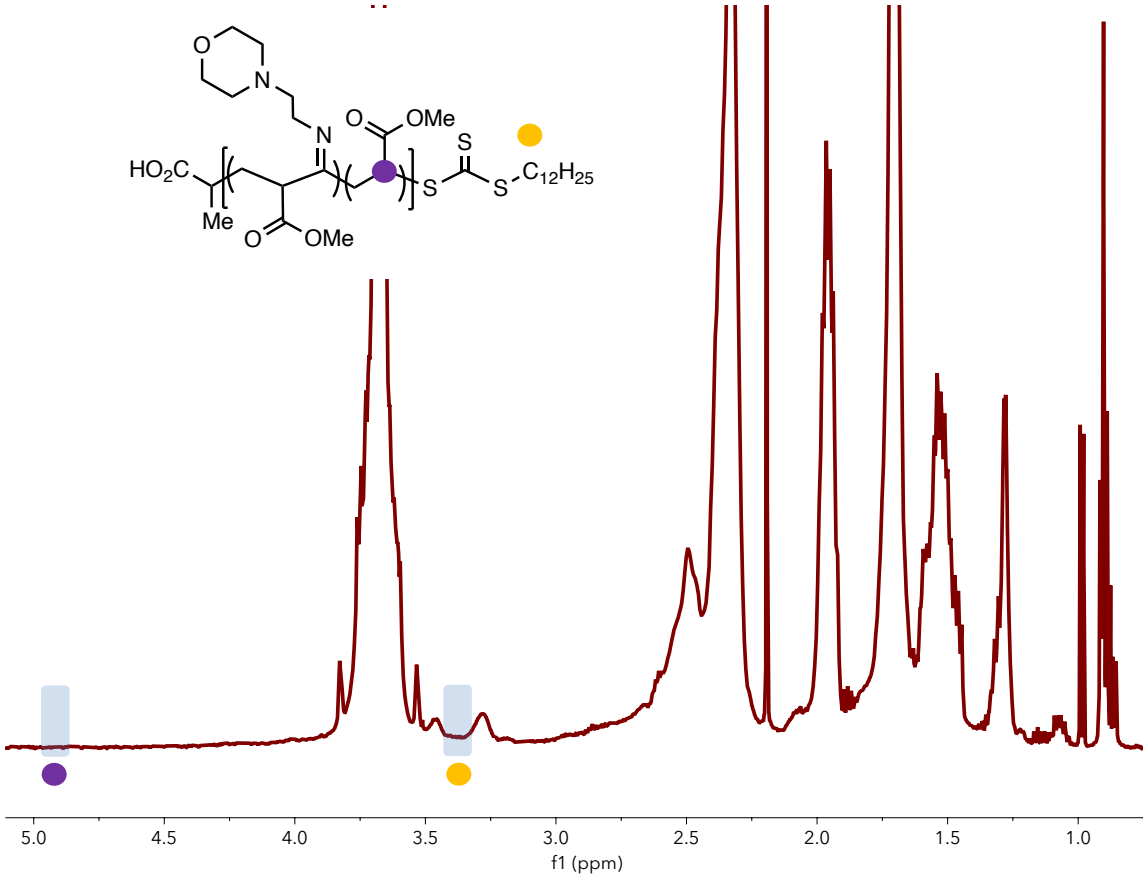

Figure 8: ^{1}H NMR of poly(MA-*co*-MEI) with no CTA peak observed

3.1.5 Control reaction studies with MEI

I undertook control reaction studies to determine why the copolymers presented high dispersities and the absence of chain end fidelity visible in ^{1}H NMR. Two four-hour reactions were completed for comparison. The first had no [Ir(dF(Me)ppy)$_2$(dtbbpy)]PF$_6$ photocatalyst (PC) and the other contained no CTA but all other reaction conditions were kept consistent. Without a PC the polymerization was slower, but I still expected to obtain the copolymer via the traditional RAFT mechanism. The absence of a photocatalyst led to no trace of copolymer detectable via GPC, and minimal conversion of MA and MEI was observed with ^{1}H NMR.

In the absence of CTA which would provide the initiating species, no polymerization was expected to occur. However, I observed high conversion of both MA and MEI, and the copolymer

possessed a high dispersity with no agreement between crude M_n and theoretical M_n (Table 6). These experiments allowed us to hypothesize that our system contained an alternative initiator activated by the PC, but this initiator was not the CTA due to large dispersities obtained.

After examining the reaction scheme and gaining insight from other photocatalytic systems, I was able to hypothesize that the iridium photocatalyst was producing an amine radical cation from the MEI monomer (Scheme 9).[23] Upon excitation with visible light, the iridium photocatalyst was reductively quenched by the tertiary amine. The resultant amine radical cation now contains a highly acidified α-C–H bond, which is easily deprotonated to afford the α-amino radical.[24] This radical species on the alkyl portion of MEI acts as an initiating species for the copolymerization.

Additionally, I performed one more control reaction where I introduced triethylamine (TEA) into the protocol in place of the isocyanide. This copolymerization between MA and TEA showed high conversion of MA, no initiating proton signal from the CTA in ^{1}H NMR, and high dispersity. Conclusively the control reactions, I was able to rationalize that the iridium photocatalyst could not be used for a controlled copolymerization of MA and MEI, so, I sought out a new photocatalyst using a photocatalyst screen.

Table 6: Control reactions to determine polymerization initiation

Deviation	M/I % conv.	M_n, crude (kg/mol)	$Đ$	M_n, theo. (kg/mol)	% incorp.	Theo. % incorp.
No PC	1.6/4.1	-	-	0.8	-	39.0%
No CTA	67/8.3	3.6	2.39	10.0	4.7%	3.0%
No MEI, TEA	>99/-	2.5	2.03	14.0	-	-

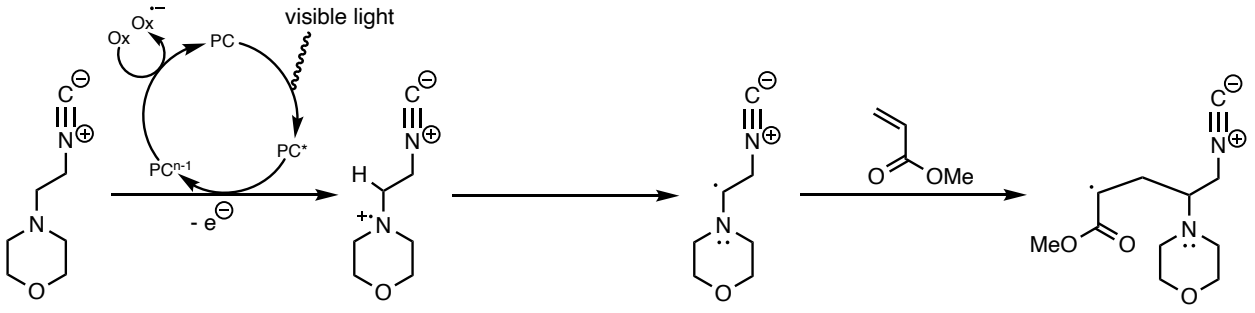

Scheme 9: Tertiary amine radical cation formation with MEI

3.1.6 Photocatalyst screening

I undertook a photocatalyst screen to assess a suitable alternative to continue PET-RAFT copolymerizations with MEI. Three photocatalysts were screened based on excited state oxidation potentials: $Ir(ppy)_3$ (4), eosin Y (5), and 4CzIPN (6) (Figure 9). The excited state oxidation potential was not calculated for MEI, however, triethylamine (TEA) exhibits an excited state oxidation potential of 0.96 V.[25] Assuming that MEI's tertiary amine would exhibit a similar oxidation potential, I attempted to target photocatalysts with excited state oxidation potentials less than 0.96 V to prevent the oxidation of MEI to the radical cation (Scheme 10).

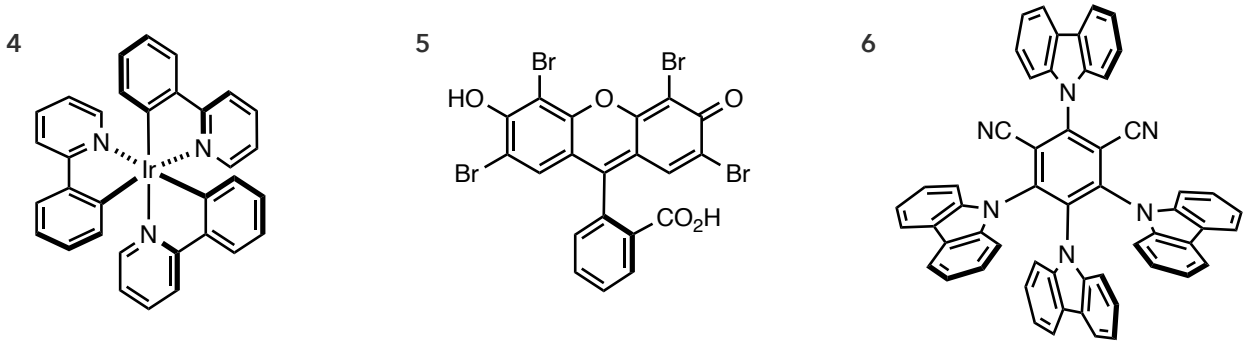

$Ir(ppy)_3$	Eosin Y	4CzIPN
Ir(III)*/Ir(IV) = -1.73 V	$E°(S/S^{-}) = -1.06$ V	$E°(S/S^{-}) = -1.18$ V
Ir(III)*/Ir(II) = 0.31 V	$E^{t}(S^*/S^{-}) = 0.79$ V	$E^{t}(S^*/S^{-}) = 1.43$ V

Figure 9: Photocatalysts screened

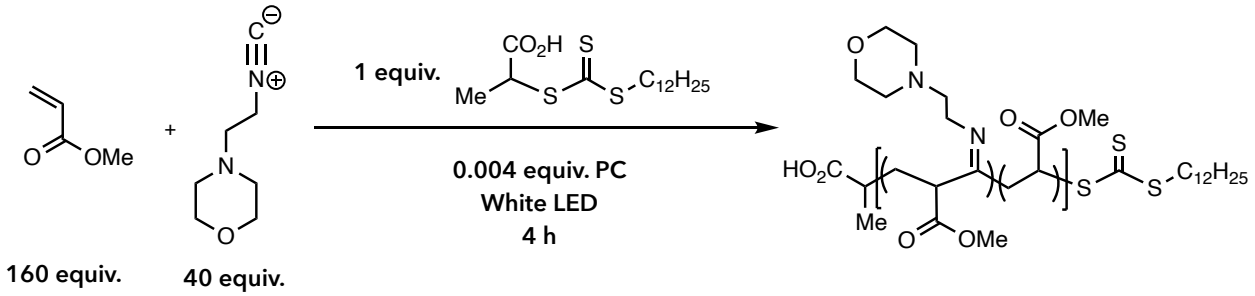

Scheme 10: Conditions for photocatalyst screen

$Ir(ppy)_3$ exhibited low monomer conversions over the 4-hour polymerization with minimal polymer produced under these conditions (Table 7 – entry 1). I had expected this photocatalyst to work well based on Boyer's pioneering research introducing PET-RAFT and because of its strong reducing potential (-1.73 V) and minimal oxidation potential (0.31 V). [26,25] However, with the data we obtained, $Ir(ppy)_3$ would require further experimentation to determine if it is viable for our system. 4CzIPN showed promising conversions of MA and MEI with initial ^{1}H NMR observations. Unfortunately, the ^{1}H NMR of the purified polymer showed no CTA peak and GPC data showed a large dispersity (Table 7 – entry 3). Originally surprised by this result, a second look at the excited state oxidation potential of 1.43 V for 4CzIPN revealed that this PC is too oxidizing for our protocol using MEI.[27]

Eosin Y (EY) as the PC exhibited acceptable monomer and isocyanide conversions and the copolymers had a dispersity less than 1.50 (Table 7 – entry 2). I was also excited to observe the CTA omega-chain end in the ^{1}H NMR spectrum of the purified polymer. This indicated the CTA controlled the propagation of the chain as expected and oxidation of the tertiary amine was not affecting control over the propagating radical. Based on this PC screening, I found that eosin Y performed the best out of the three photocatalysts tested and could be used for further light induced copolymerizations with MEI.

Table 7: PC screen - conversion, molecular weight, and incorporation data

Entry	Photocat.	M/I % conv.	M_n, crude (kg/mol)	$Đ$	M_n, theo. (kg/mol)	% incorp.
1	$Ir(ppy)_3$	4/4	1.9	1.14	1.1	-
2	eosin Y	38/7	5.3	1.41	6.0	4.8%
3	4CzIPN	82/14	5.1	2.30	12.4	5.5%

3.1.7 Light screening with eosin Y

Previously, I had employed white LEDs when obtaining poly(MA-*co*-TosMIC) and for the PC screening. I aimed to optimize the conditions when using EY, so, various light sources were screened (Scheme 11). Literature UV-vis data for eosin Y showed a maximum absorbance at 525 nm with continued absorbance into the blue region of the light spectra.[28,29] Green light provided the best control over the dispersity of the polymers over a 4 hour polymerization. However, continued efforts with green LED light did not provide a desirable yield of polymer after purification (Table 8 – Entries 2-4). Notably, a Kessil light source producing 456 nm light at 50% power provided higher conversion, more polymer, and low dispersity (Table 8 – Entry 5).

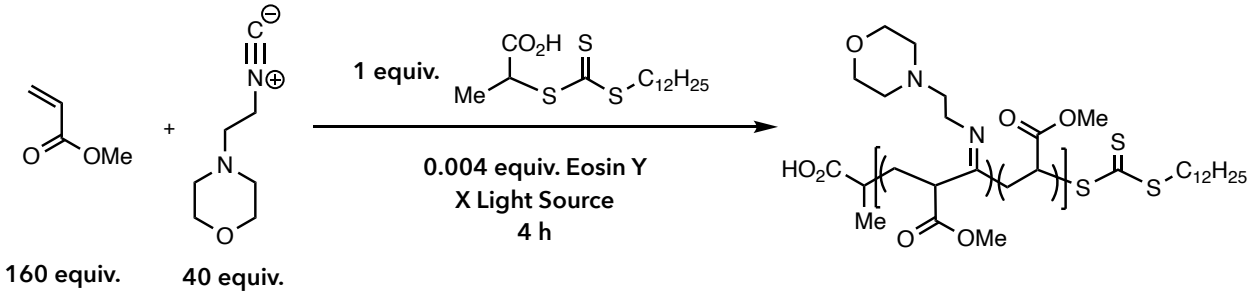

Scheme 11: Conditions for light source screening with eosin Y

Table 8: Light source screen

Entry	Light	M/I % conv.	M_n, crude (kg/mol)	$Đ$	M_n, theo. (kg/mol)	% incorp.
1	White LED	38/7	5.3	1.41	6.0	4.8%
2	Green LED	18/5	3.1	1.26	3.1	4.4%
3	525 nm LED	24/5	3.3	1.26	3.9	4.2%
4	525 nm Kessil	18/4	2.8	1.27	3.1	4.0%
5	456 nm Kessil (50%)	40/6	5.5	1.38	6.2	3.9%

To determine a suitable light source, I continued to control reactions to optimize conditions using EY as our PC. Polymerizations of MA were completed using green LEDs and 456 nm light at 50% power (Scheme 12). When I attempted to polymerize MA to PMA, the green LED light source was not effectively able to polymerize MA (Table 9 – entry 1), even after twenty-four hours (Table 9 – entry 2). This was unexpected but led to new insight with EY.

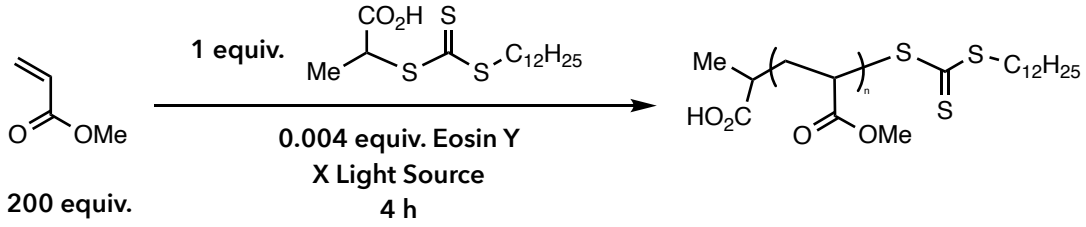

Scheme 12: Polymerization of MA for light source screen

Table 9: Polymerization of MA with EY as the PC

Entry	Light	Variation	MA % conv.	M_n, crude (kg/mol)	$Đ$
1	Green LED	-	1.0	0.83	1.03
2	Green LED – 24 h	-	1.0	0.85	1.03
3	456 nm Kessil (50%)	-	96	11.1	1.21
4	456 nm Kessil (50%)	No PC	93	10.7	1.16

Again, I had expected EY to work well with green light based on its UV-vis maximum absorbance at 525 nm, so, further investigation into the background of EY as a PC was

required.[28,29] Through the research I conducted on EY I uncovered that the PC exists as both a monomer and dimer when in solution.[30, 31] However, the dimeric form dominates in solution owed to hydrogen bonding.[31] Alvarez-Martin and coworkers reported that longer wavelengths of light cause eosin Y to degrade faster than shorter wavelengths of light. They also reported that a light degraded intermediates alter the hue of the solution causing it to be less susceptible to green light.[31]

To observe this in my polymerization of MA, I set up a control where I measured the absorbance of the solution using UV-vis prior to and then post irradiation with green LEDs (Figure 10). There was a dramatic decrease in intensity of the green light absorbance band, but the blue absorbance band remained constant. Visually, I also saw a dramatic color change with my polymerizations. Prior to irradiation, the solution would be brilliant red, but after irradiation a pale-yellow color was observed. Fortunately, EY and the degraded intermediates still absorbed under blue light based on the UV-vis and from data reported in literature.[31] I was able to confirm that blue light (456 nm) could be used to effectively polymerizing MA using EY as the PC (Table 9 – entry 3).

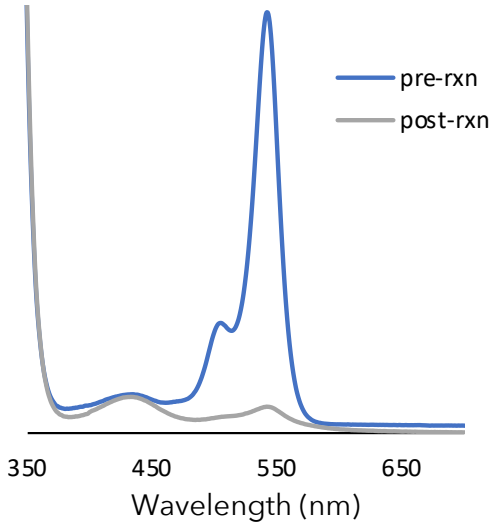

Figure 10: UV-vis of the reaction before and post irradiation

Prior to moving forward with optimal condition employing blue light to excite EY, I

executed one additional experiment to rule out photo-iniferter RAFT polymerization (Table 9 – entry 4).[32] This was conducted without the EY photocatalyst to determine if light could directly excite the CTA to initiate, transfer propagating chains, and terminate the polymerization in a controlled manner via the RAFT equilibrium.[22,32] Based on the conversion and GPC results shown in Table 9 – entry 4, I concluded that the polymerization of MA using 456 nm light did occur via PI-RAFT. Noteworthy though, with EY present in solution as a PC, I did observe a higher conversion of MA (Table 9 – entries 3 & 4). I also hypothesized that when a comonomer such as an isocyanide is introduced, the addition of a PC would be essential to boost the polymerization rates based off the MA and TosMIC kinetics previously reported. Based on this hypothesis, I concluded that 456 nm light should be used for our copolymerizations to ensure less byproduct formation and continued excitation of the EY as it is irradiated when in the presence of MEI.[30]

3.1.8 Fluorescence quenching studies

Moving forward, I wanted to provide secondary evidence to confirm MEI wasn't being oxidized to the radical cation by obtaining fluorescence quenching data of EY. PET-RAFT systems effectively employ light in the visible or UV spectra to excite a PC, permit an electron transfer, and reduce the CTA.[26] When there isn't a species present in solution for the electron transfer from the photocatalysts excited state, the PC returns to the ground state by emitting the energy in the form of light.[33] The light released is fluorescence, which can be monitored using a fluorescence spectrometer.[33] This instrument can obtain the intensity of fluorescence by exciting a molecule at a specified wavelength of light to induce fluorescence and records how it emits light the visible or UV spectra. The emission maximum, or intensity apex of the fluorescence spectra, can decrease if a quencher is present within a solution providing useful data when analyzing complex environments. By introducing different concentrations of quenchers and comparing these to a

control with no quencher, a Stern-Volmer plot can be created to determine how fast a species might be quenching a fluorescing molecule.

I examined both EY and $[Ir(dF(Me)ppy)_2(dtbbpy)]PF_6$ (denoted in this study as Ir(Me)) for quenching with MEI and CTA (Figure 11 – graph A). The samples were excited at 456 nm light and the emission max was recorded for the various quencher concentrations tested. I hypothesized that the CTA would quench the excited state of EY, rather than MEI. The Stern-Volmer relationship I plotted showed that the CTA did effectively quench the excited state of EY, while MEI did not quench EY. We were able to draw this conclusion from Figure 11 – graph A because the positive slope indicated that the emission maximum decreased as the concentration of CTA, the quencher, was increased.

To complete this study, I observed how $[Ir(dF(Me)ppy)_2(dtbbpy)]PF_6$ quenched in the presence of MEI and the CTA. Based on my hypothesis that an iridium PC generated a radial cation when MEI was present, I expected the iridium PC to quench in the presence of MEI producing a Stern-Volmer plot with a positive slope. I also anticipated the CTA to quench the iridium PC and hoped to gain insight as to which component would quench the iridium PC faster. The data I obtained for quenching the iridium PC with MEI did graph with a positive slope (Figure 11 – graph A), but not as dramatically as the slope graphed with the PC quenched by CTA (Figure 11 – graph B). This confirmed the first hypothesis and provided evidence that even with MEI present, the CTA can still be reduced by an iridium PC. Overall, the EY photocatalyst system shows that when exciting it with 456 nm light, the excited state of EY will be quenched by reducing the CTA, which will initiate polymerization and control the propagating chains.

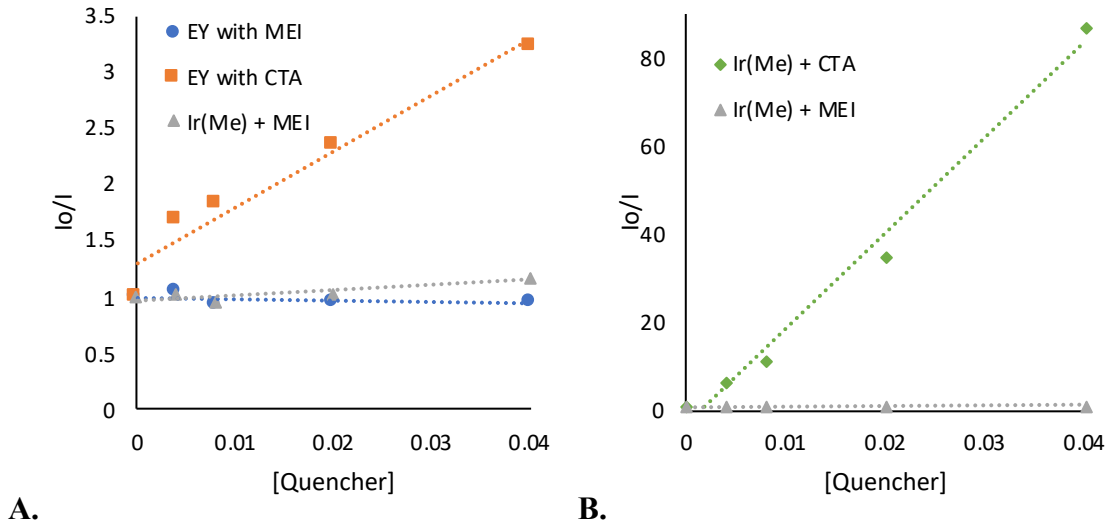

Figure 11: Stern-Volmer plots. A. MEI does quench Ir(Me) PC but does not quench EY. CTA does quench EY as desired. B. CTA quenched Ir(Me) more than MEI.

3.1.9 Varying the incorporation of MEI with MA

With the new insight gained from the control reactions, PC screen, light screen, and fluorescence quenching studies, I proposed new reaction conditions to obtain poly(MA-*co*-MEI) (Scheme 13). As completed for the previous experiments, I varied the feed ratios to tune the incorporation of isocyanide. I expected to obtain higher conversions than previously seen with green LEDs while maintaining dispersities less than 1.50. The results in Table 9 provided the evidence that we expected for these copolymerizations. Also, ^{1}H NMR showed the desired proton peaks at 3.37 ppm and 4.90 ppm indicating that CTA controlled the propagation of the copolymer chains. These reaction conditions were also able to produce polymers with tunable incorporations of MEI from 1.7% to 5.9% (Table 10).

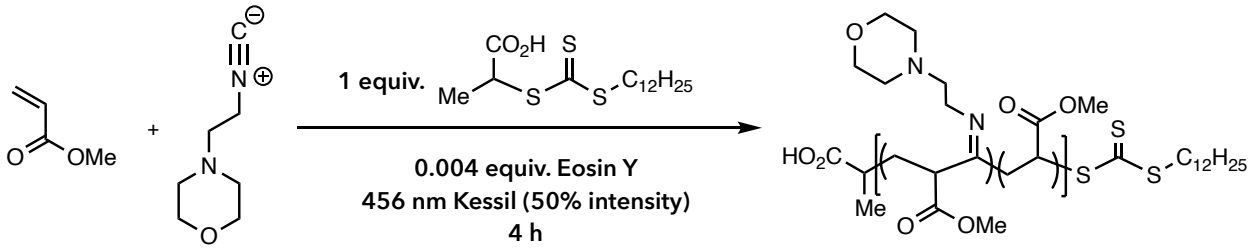

Scheme 13: Optimized PET-RAFT conditions to obtain poly(MA-*co*-MEI)

Table 10: Tunable incorporations and control over poly(MA-*co*-MEI)

Feed Ratio	M/I % conv.	M_n, crude (kg/mol)	$Đ$	M_n, theo. (kg/mol)	% incorp.	Theo. % incorp.
180:20	43/7	5.4	1.25	7.2	1.7%	1.7%
160:40	40/6	5.5	1.38	6.2	3.9%	3.6%
140:60	30/5	4.4	1.42	4.4	5.9%	6.7%

Now that I had conditions to obtain the copolymers, kinetic studies for this system were completed to gain insight in MA and isocyanide conversion over time (Figure 12). Typically, the data collected would include up to 80% MA conversion, however, due to time constraints, the conversion of MA after six hours only reached 60%. Future kinetic studies for this system will include data targeting higher conversion of both MA and MEI. The data the I was able to obtain showed a linear increase in conversion over time for both MA and MEI. This was promising and future work will hopefully provide more information of the copolymerization kinetics to draw conclusions when comparing the kinetics of copolymerizing MA with TosMIC.

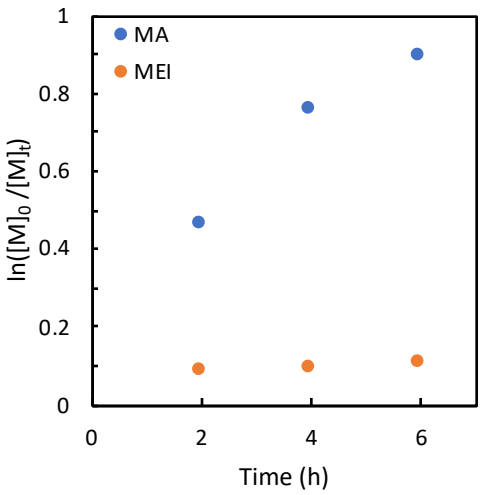

Figure 12: Kinetics of MA and MEI copolymerization

Finally, I wanted to ensure that I could copolymerize MA with TosMIC using EY as the PC (Scheme 14). This data was collected and compared to the standard conditions previously used in Scheme 2. I varied the feed ratios to tune the TosMIC incorporation from 2.2% to 8.1% (Table 11), which was close to the incorporations obtained via the standard reaction conditions (Table 2). The new protocol with EY produced copolymers with similar molecular weights with lower dispersities than the previous system with the Ir(Me) PC (Table 2 & 11).

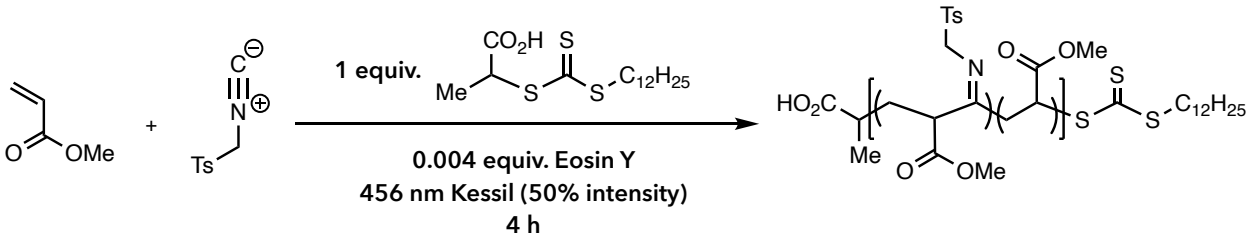

Scheme 14: Conditions to obtain poly(MA-*co*-TosMIC) with EY as the PC

Table 11: Poly(MA-*co*-TosMIC) data obtained with EY as a PC

Feed Ratio	M/I % conv.	M_n, crude (kg/mol)	$Đ$	M_n, theo. (kg/mol)	% incorp.	Theo. % incorp.
180:20	46/13	4.7	1.25	8.0	2.2%	3.0%
160:40	33/11	3.2	1.25	5.8	4.4%	7.7%
140:60	40/16	3.1	1.39	7.0	8.1%	14.6%

A goal I had while executing these experiments was to gain insight into copolymerizing different types of isocyanides. The method I used to synthesize poly(MA-*co*-MEI) with the alkyl isocyanide produced copolymers that were larger, but these copolymers exhibited less incorporation of MEI within the polymer backbone. When I utilized EY and 456 nm light to obtain poly(MA-*co*-TosMIC) the copolymers showed low dispersities possibly indicating that the strong electron withdrawing nature of the tosyl group stabilized the imidoyl radical formed, whereas MEI did not have the capability as an alkyl isocyanide. I believe this to be similar to the stability observed with more activated monomers (MAMs), which have stabilization of a radical species through conjugation. Thanks to the insight and the success seen with this data, I continued expanding the scope of the copolymerizations to include additional monomers.

4.1 Expanding the monomer scope to include vinyl acetate

4.1.1 Introduction to less activated monomers (LAMs)

The discrete Co-H initiated CMRP polymerization conditions are unable to initiate vinyl acetate (VAc) polymerization.[19] PET-RAFT was chosen to broaden the monomer scope to include these and other monomer which can be polymerized via this method. The CTA controlling the RAFT equilibrium can be designed to initiate and propagate a broad scope of monomers, whether they are less or more activated. More activated monomers possess conjugation to stabilize the radical species formed while less activate monomers have very reactive radicals that are not stabilized through conjugation.

CTA design for less activated monomers requires that the intermediate radical formed to be less stable, this favors fragmentation of the propagating radical. By adding a nitrogen, present in dithiocarbamate CTAs, it can delocalize its lone pair of electrons to the thiocarbonyl group. This deactivates the carbon-sulfur double bond towards radical addition and promotes fragmentation of the propagating radical. I synthesized the CTA (9) found in Scheme 15 to control the polymerization of vinyl acetate via PET-RAFT.

4.1.2 Conditions to copolymerize VAc with isocyanides

I modified the conditions used to obtain the previous copolymers with MA to reflect the new conditions required to copolymerize VAc with the isocyanides using the newly synthesize CTA. I targeted a DP of 200 for the VAc and isocyanide copolymers and attempted to tune the incorporations of the isocyanides by modifying the feed ratios. The protocol I utilized to access poly(VAc-*co*-TosMIC) was unsuccessful (Scheme 15). However, the protocol to obtain poly(VAc-*co*-MEI) was successful (Scheme 16). The ^{1}H NMRs obtained when I targeted three different feed ratios exhibited an increased intensity as higher incorporations of MEI were targeted.

GPC helped confirmed I was obtaining copolymers based on the M_n. I observed the chain ends of the CTA in ^{1}H NMR and low dispersities indicating that the CTA maintained control over monomer propagation. Although polymerization achieved and incorporation was evident in the ^{1}H NMR, I needed to further investigate the spectra to calculate the incorporation of MEI (Figure 13).

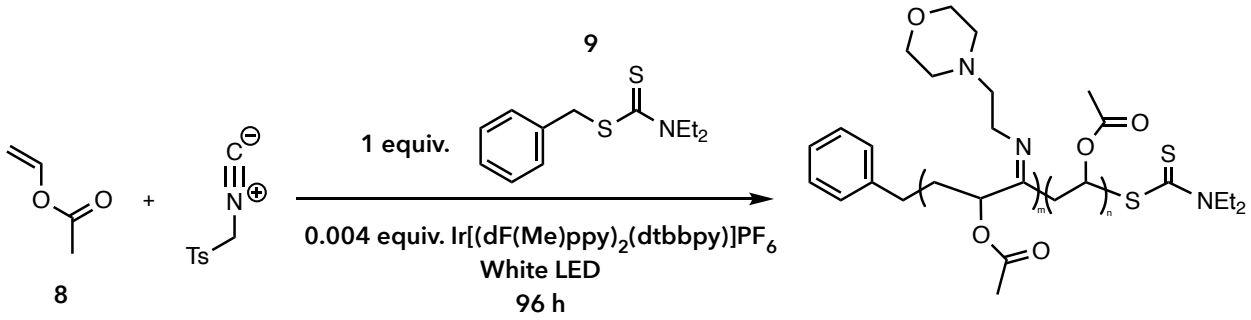

Scheme 15: Conditions for VAc and TosMIC copolymerization

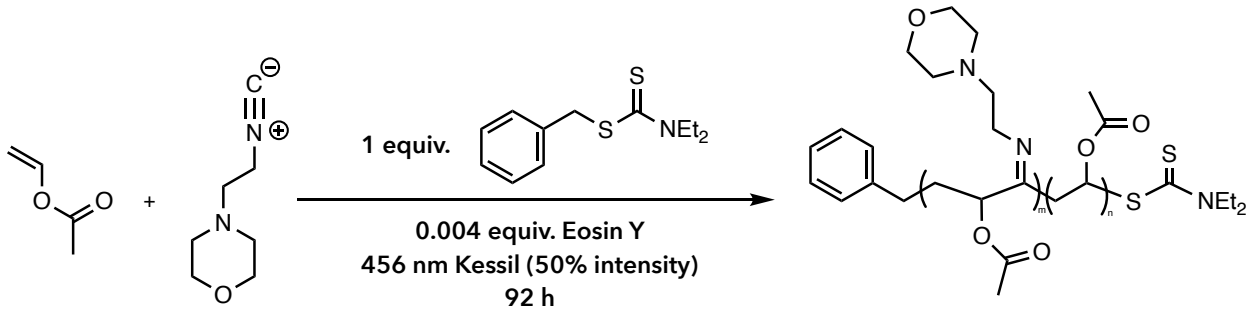

Scheme 16: Conditions for VAc and MEI copolymerization

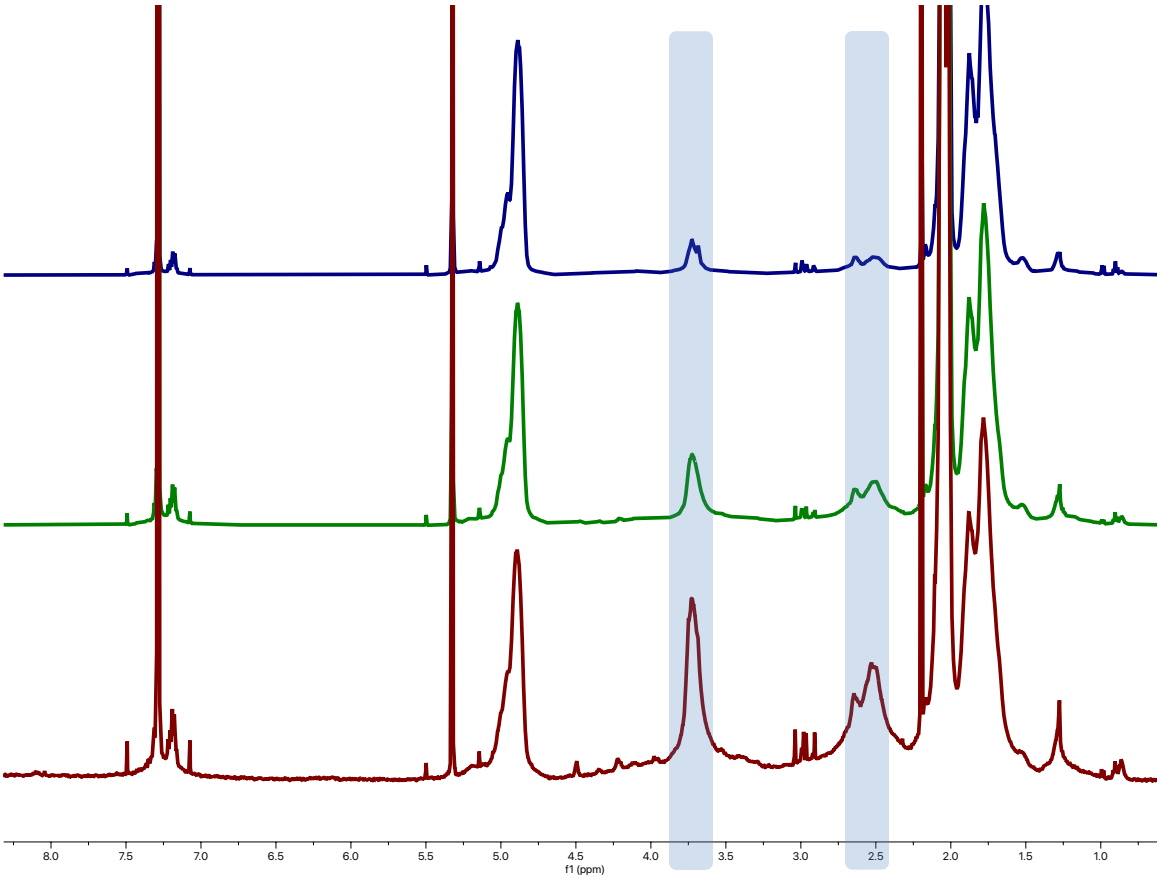

Figure 13: ^{1}H NMR showed tunable MEI incorporations with VAc

Table 12: Poly(VAc-*co*-MEI) tunable incorporation of MEI

Feed Ratio	M_n, pure (kg/mol)	$Đ$	% incorp.
190:10	4.5	1.47	3.1%
180:20	3.7	1.36	6.8%
170:30	2.7	1.3	16.2%

4.1.3 Investigating MEI incorporation

To determine the incorporation of MEI, I integrated the expected proton shifts that corresponded to MEI and revealed an equal ratio of protons with the signals that correspond to MEI's microstructure. The signal downfield at 3.7 ppm matched with the protons around the morpholino oxygen and the two protons closest to the imine, while the peak at 2.5 ppm corresponds to the six protons directly adjacent to the tertiary amine (Figure 14).

These polymers do not possess the conjugation discovered with the poly(MA-*co*-isocyanide) copolymers, therefore, they don't tautomerize, and are conformationally locked with the imine in the backbone. By integrating the VAc peak at 4.9 ppm to one, I was able to formulate an equation to calculate the percentage of MEI incorporated into the backbone of the copolymer (Equation 3). The copolymers I synthesized exhibited incorporations of MEI from 3.1% to 16.2% (Table 12). These copolymers indicated that I could gain higher incorporations of MEI with VAc in comparison to MA. I have hypothesized that the imidoyl radical is potentially more kinetically favored during propagation providing access to higher incorporations at lower feed ratios, but additional research investigating the mechanism through kinetics and reactivity ratios will be required to gain more insight.

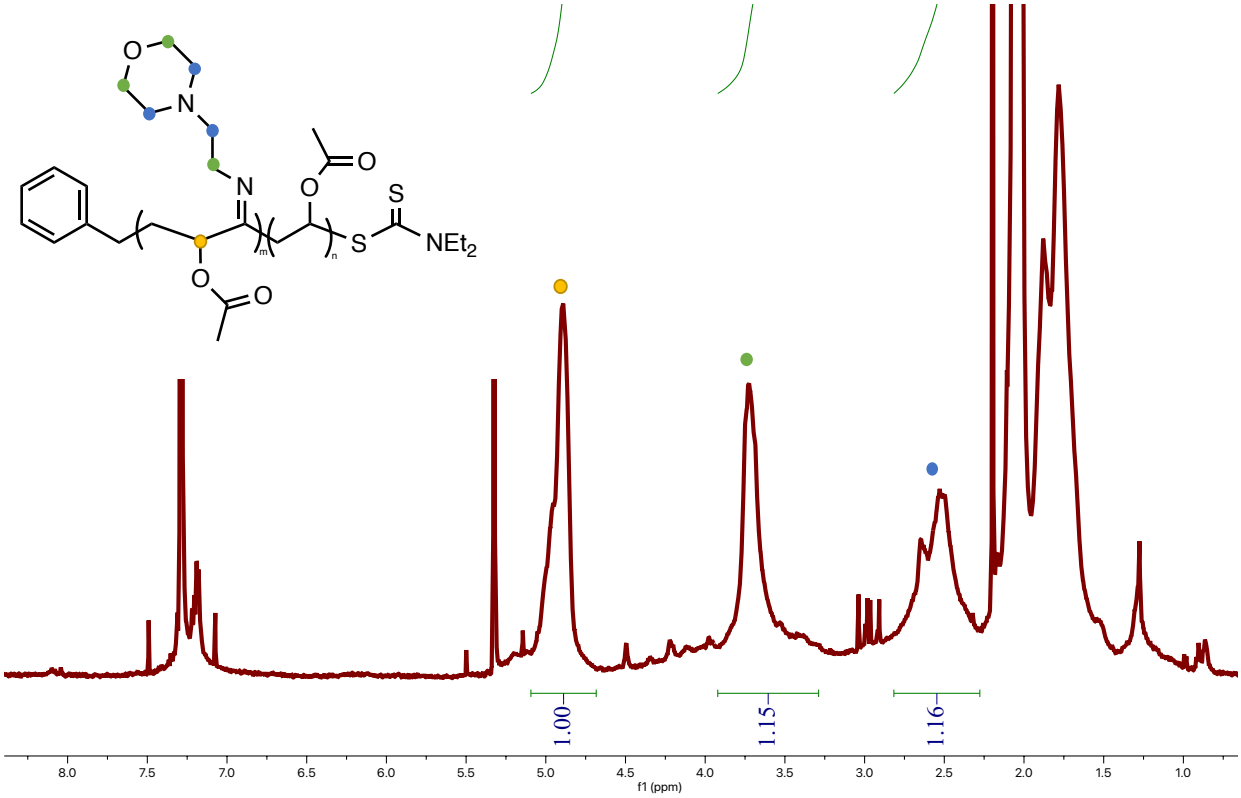

Figure 14: ^{1}H NMR integrated to show incorporation of MEI

$$\% \, MEI \; incorp. = \frac{\left({}^{1}/_{6} * MEI \; methylene \; protons \; adjacent \; to \; tertiary \; amine \right)}{(1 \; Vinyl \; Acetate \; proton) + \left({}^{1}/_{6} * MEI \; methylene \; protons \; adjacent \; to \; tertiary \; amine\right)}$$

Equation 3

5.1 Post-polymerization modifications

5.1.1 Hydrolysis of poly(MA-*co*-TosMIC) to afford poly(MA-*co*-ketone)

The Stache group previously reported hydrolysis of their TosMIC incorporated copolymers to afford the desired carbonyl within the backbone. I followed their established conditions using water and catalytic acid to confirm I could hydrolyze TosMIC from the copolymers to afford the carbonyl (Scheme 17). The disappearance of TosMIC's methylene and enamine protons seen in the ^{1}H NMR (Figure 15 - A) provided evidence that I was successfully able to employ the conditions found in Scheme 17 to afford poly(MA-*co*-ketone) (Figure 15 - B). The newly formed copolymer should be susceptible to Norrish Type reactions to afford monomer and oligomer moieties, establishing a unique chemical recycling path for these copolymers as observed with the Stache groups previous work.

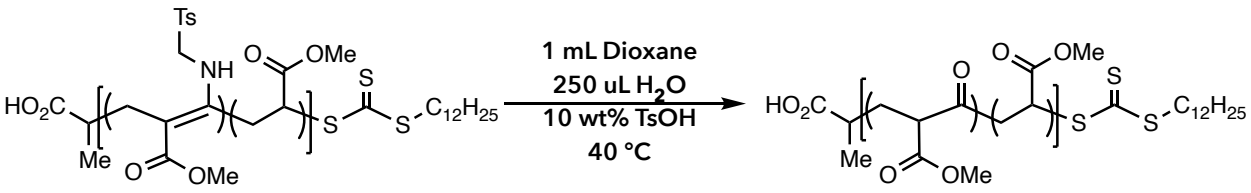

Scheme 17: Hydrolysis conditions to obtain carbonyls along the backbone

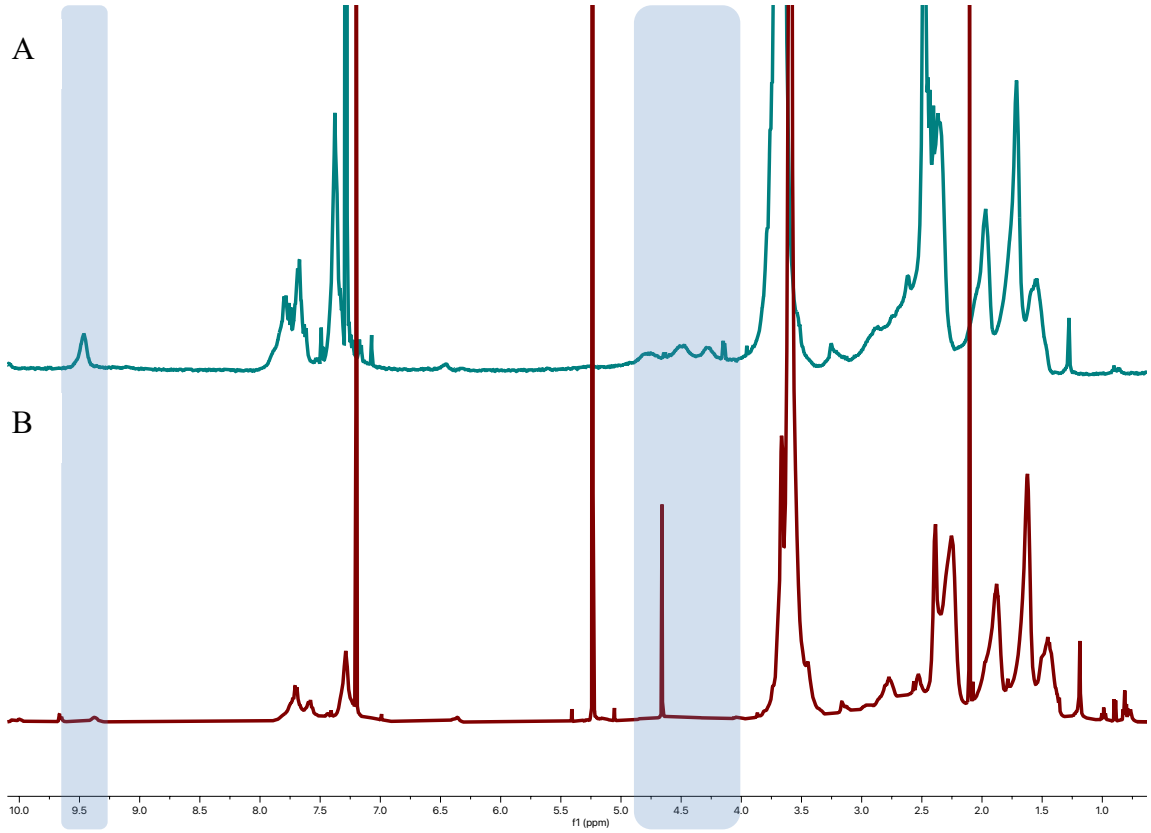

Figure 15: Hydrolysis of poly(MA-*co*-TosMIC) (A) to afford poly(MA-*co*-ketone) (B)

5.1.2 Condensation with amines

Additionally, I attempted post-polymerization modifications to condense amines onto the poly(MA-*co*-ketone) copolymers. Based off of work done by the Sumerlin group, I envisioned functionalizing the poly(MA-*co*-ketone) copolymers with primary amines or diamines to afford polymers and crosslinked polymers with unique thermal and physical properties.[34] The diamine would allow access to crosslinked materials, creating unique networks which I envisioned could be reprocessed via hydrolysis gaining access to a potential chemical recycling avenue. Sumerlin's group was able to provide evidence of this with their vitrimer networks they synthesized, showing that they could reprocess their material up to three times while maintaining desirable properties.[35] I attempted functionalizing the poly(MA-*co*-ketone) copolymers with primary amines following the conditions set in Scheme 18. Unfortunately, these preliminary attempts were unsuccessful but

with further study, I could envision future research to succeed in these prospects.

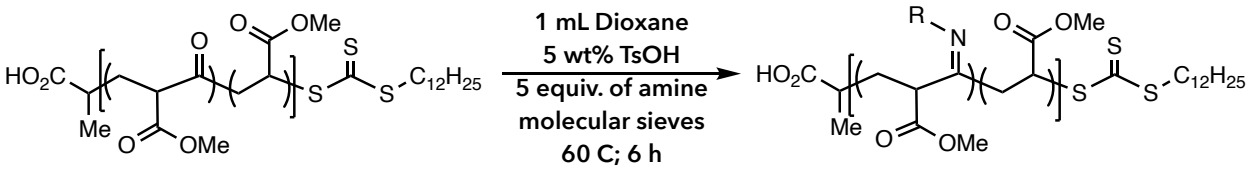

Scheme 18: Amine condensation conditions

6.1 Conclusions

In this work, I have described the methods behind obtaining novel copolymers containing tunable incorporations of isocyanides with both methyl acrylate and vinyl acetate monomers using PET-RAFT. I was able to show that this method can be used to obtain poly(MA-*co*-TosMIC) with tunable incorporations of TosMIC. The tautomerization seen in the Stache group's Co-H CMRP system was observed with the copolymers obtained with this method as well, which may help give further insight into the other desirable microstructures for this copolymer. Through tautomerization I showed the proposed mechanism of the lactam formation. Future work can be done to drive the conformational change to the lactam, which will introduce rigidity into the backbone of the polymer most likely increasing the thermal properties.

Next, I provided evidence that I could overcome the initial challenges presented in the first set of conditions that were used to obtain poly(MA-*co*-MEI). Eliminations through catalyst and light source screening provided the appropriate conditions to tune the incorporation of MEI with MA using eosin Y as the photocatalyst and 456 nm light. These polymers showed chain end fidelity and presented low dispersities. I also used NMR and MestReNova NMR prediction software to elucidate the microstructure of poly(MA-*co*-MEI).

To complete this study with MA and isocyanides, I copolymerized MA and TosMIC using the conditions designed for MA and MEI. This data gave insight into the possible differences for incorporation mechanism when copolymerizing with an aromatic versus an alkyl isocyanide. With further studies and more isocyanides, the hypothesis could be validated where I believed that the aromatic isocyanides help to stabilize the imidoyl radical formed favoring monomer propagation.

Utilizing the knowledge that I obtained with the previous copolymerizations, I implemented conditions to access poly(VAc-*co*-MEI) through CTA. These copolymers also

showed tunable incorporation evident in ^{1}H NMR, and I used the spectra to calculate the isocyanide incorporations. Further studies could investigate CTA design to help facilitate the copolymerization with TosMIC or another aromatic isocyanide. Additional feed ratios should also be targeted for this system to obtain kinetic data for the propagation of both VAc and MEI to gain further insight into the mechanism.

Finally, I was able to show that I could hydrolyze poly(MA-*co*-TosMIC) to afford poly(MA-*co*-ketone). Future work within this part of the project will include expanding the hydrolysis to include poly(MA-*co*-MEI). The thermal properties of the polymers before and after hydrolysis using differential scanning calorimetry (DSC) can be measured and I could use the Stache group's photodegradation protocol to investigate photodegradability of these copolymers. Applying the hydrolysis conditions to our vinyl acetate copolymers will afford poly(vinyl alcohol-*co*-ketone) copolymers.[36] This might also be a potential avenue for this project when observing the copolymer properties.

Future directions for this work, including ideas stated above, will potentially feature additional monomers and isocyanides. Gaining insight in copolymer properties with additional monomers will provide knowledge on potential application capabilities of these copolymers industrially. We can then envision all the possibilities of obtaining recyclable vitrimers accessed by crosslinking our novel copolymers, aiming for ways to access a more sustainable future through chemical recycling of commercial polymers.

BIBLIOGRAPHY

(1) *History and Future of Plastics*. Science History Institute. https://sciencehistory.org/education/classroom-activities/role-playing-games/case-of-plastics/history-and-future-of-plastics/ (accessed 2023-07-01).

(2) Chamas, A.; Moon, H.; Zheng, J.; Qiu, Y.; Tabassum, T.; Jang, J. H.; Abu-Omar, M.; Scott, S. L.; Suh, S. Degradation Rates of Plastics in the Environment. *ACS Sustain. Chem. Eng.* **2020**, *8* (9), 3494–3511. https://doi.org/10.1021/acssuschemeng.9b06635.

(3) OECD. *Global Plastics Outlook: Economic Drivers, Environmental Impacts and Policy Options*; OECD, 2022. https://doi.org/10.1787/de747aef-en.

(4) *Plastics and the circular economy*. https://emf-digital.shorthandstories.com/plastics-and-the-circular-economy/ (accessed 2023-07-02).

(5) Göktürk, E.; Pemba, A. G.; Miller, S. A. Polyglycolic Acid from the Direct Polymerization of Renewable C1 Feedstocks. *Polym. Chem.* **2015**, *6* (21), 3918–3925. https://doi.org/10.1039/C5PY00230C.

(6) Li, K.; Tian, S.; Zhao, Y. Polymer Degradation and Degradable Polymer Designing. In *2021 3rd International Academic Exchange Conference on Science and Technology Innovation (IAECST)*; 2021; pp 1217–1222. https://doi.org/10.1109/IAECST54258.2021.9695776.

(7) Vavasori, A.; Ronchin, L. Polyketones: Synthesis and Applications. In *Encyclopedia of Polymer Science and Technology*; John Wiley & Sons, Ltd, 2017; pp 1–41. https://doi.org/10.1002/0471440264.pst273.pub2.

(8) Yang, Y.; Li, S.-Y.; Bao, R.-Y.; Liu, Z.-Y.; Yang, M.-B.; Tan, C.-B.; Yang, W. Progress in Polyketone Materials: Blends and Composites. *Polym. Int.* **2018**, *67* (11), 1478–1487. https://doi.org/10.1002/pi.5624.

(9) Drent, E.; Mul, W. P.; Smaardijk, A. A. Polyketones. In *Encyclopedia of Polymer Science and Technology*; John Wiley & Sons, Ltd, 2001. https://doi.org/10.1002/0471440264.pst273.

(10) Drent, E.; Budzelaar, P. H. M. Palladium-Catalyzed Alternating Copolymerization of Alkenes and Carbon Monoxide. *Chem. Rev.* **1996**, *96* (2), 663–682. https://doi.org/10.1021/cr940282j.

(11) Soomro, S. S.; Cozzula, D.; Leitner, W.; Vogt, H.; Müller, T. E. The Microstructure and Melt Properties of CO–Ethylene Copolymers with Remarkably Low CO Content. *Polym. Chem.* **2014**, *5* (12), 3831–3837. https://doi.org/10.1039/C3PY01637D.

(12) Luo, R.; Newsham, D. K.; Sen, A. Palladium-Catalyzed Nonalternating Copolymerization of Ethene and Carbon Monoxide: Scope and Mechanism. *Organometallics* **2009**, *28* (24), 6994–7000. https://doi.org/10.1021/om9008235.

(13) Arrington, K. J.; Murray, C. B.; Smith, E. C.; Marand, H.; Matson, J. B. Precision Polyketones by Ring-Opening Metathesis Polymerization: Effects of Regular and Irregular Ketone Spacing. *Macromolecules* **2016**, *49* (10), 3655–3662. https://doi.org/10.1021/acs.macromol.6b00590.

(14) Morgen, T. O.; Baur, M.; Göttker-Schnetmann, I.; Mecking, S. Photodegradable Branched Polyethylenes from Carbon Monoxide Copolymerization under Benign Conditions. *Nat. Commun.* **2020**, *11* (1), 3693. https://doi.org/10.1038/s41467-020-17542-5.

(15) Chen, S.-Y.; Pan, R.-C.; Chen, M.; Liu, Y.; Chen, C.; Lu, X.-B. Synthesis of Nonalternating Polyketones Using Cationic Diphosphazane Monoxide-Palladium Complexes. *J. Am. Chem. Soc.* **2021**, *143* (28), 10743–10750. https://doi.org/10.1021/jacs.1c04964.

(16) Tang, S.; Seidel, F. W.; Nozaki, K. High Density Polyethylenes Bearing Isolated In-Chain Carbonyls**. *Angew. Chem. Int. Ed.* **2021**, *60* (51), 26506–26510. https://doi.org/10.1002/anie.202110957.

(17) Voccia, M.; Odenwald, L.; Baur, M.; Lin, F.; Falivene, L.; Mecking, S.; Caporaso, L. Mechanistic Insights into Ni(II)-Catalyzed Nonalternating Ethylene–Carbon Monoxide Copolymerization. *J. Am. Chem. Soc.* **2022**, *144* (33), 15111–15117. https://doi.org/10.1021/jacs.2c04563.

(18) Camdzic, L.; Stache, E. E. Controlled Radical Polymerization of Acrylates and Isocyanides Installs Degradable Functionality into Novel Copolymers. *submitted*.

(19) Dadashi-Silab, S.; Stache, E. E. A Hydrometalation Initiation Mechanism via a Discrete Cobalt-Hydride for a Rapid and Controlled Radical Polymerization. *J. Am. Chem. Soc.* **2022**, *144* (29), 13311–13318. https://doi.org/10.1021/jacs.2c04655.

(20) Perrier, S. 50th Anniversary Perspective: RAFT Polymerization—A User Guide. *Macromolecules* **2017**, *50* (19), 7433–7447. https://doi.org/10.1021/acs.macromol.7b00767.

(21) Xu, J.; Jung, K.; Atme, A.; Shanmugam, S.; Boyer, C. A Robust and Versatile Photoinduced Living Polymerization of Conjugated and Unconjugated Monomers and Its Oxygen Tolerance. *J. Am. Chem. Soc.* **2014**, *136* (14), 5508–5519. https://doi.org/10.1021/ja501745g.

(22) Allegrezza, M. L.; Konkolewicz, D. PET-RAFT Polymerization: Mechanistic Perspectives for Future Materials. *ACS Macro Lett.* **2021**, *10* (4), 433–446. https://doi.org/10.1021/acsmacrolett.1c00046.

(23) Hu, J.; Wang, J.; Nguyen, T. H.; Zheng, N. The Chemistry of Amine Radical Cations Produced by Visible Light Photoredox Catalysis. *Beilstein J. Org. Chem.* **2013**, *9*, 1977–2001. https://doi.org/10.3762/bjoc.9.234.

(24) Beatty, J. W.; Stephenson, C. R. J. Amine Functionalization via Oxidative Photoredox Catalysis: Methodology Development and Complex Molecule Synthesis. *Acc. Chem. Res.* **2015**, *48* (5), 1474–1484. https://doi.org/10.1021/acs.accounts.5b00068.

(25) Merck-Photocatalysis-Chart.Pdf. https://macmillan1.wpengine.com/wp-content/uploads/Merck-Photocatalysis-Chart.pdf (accessed 2023-06-30).

(26) Shanmugam, S.; Xu, J.; Boyer, C. Photoinduced Electron Transfer–Reversible Addition–Fragmentation Chain Transfer (PET-RAFT) Polymerization of Vinyl Acetate and N-Vinylpyrrolidinone: Kinetic and Oxygen Tolerance Study. *Macromolecules* **2014**, *47*, 4930–4942. https://doi.org/10.1021/ma500842u.

(27) Speckmeier, E.; Fischer, T. G.; Zeitler, K. A Toolbox Approach To Construct Broadly Applicable Metal-Free Catalysts for Photoredox Chemistry: Deliberate Tuning of Redox Potentials and Importance of Halogens in Donor–Acceptor Cyanoarenes. *J. Am. Chem. Soc.* **2018**, *140* (45), 15353–15365. https://doi.org/10.1021/jacs.8b08933.

(28) *Eosin Y*. https://omlc.org/spectra/PhotochemCAD/html/061.html (accessed 2023-06-30).

(29) Majek, M.; Filace, F.; Wangelin, A. J. V. On the Mechanism of Photocatalytic Reactions with Eosin Y. *Beilstein J. Org. Chem.* **2014**, *10*, 981–989. https://doi.org/10.3762/bjoc.10.97.

(30) Chakraborty, M.; Panda, A. K. Spectral Behaviour of Eosin Y in Different Solvents and Aqueous Surfactant Media. *Spectrochim. Acta. A. Mol. Biomol. Spectrosc.* **2011**, *81* (1), 458–465. https://doi.org/10.1016/j.saa.2011.06.038.

(31) Alvarez-Martin, A.; Trashin, S.; Cuykx, M.; Covaci, A.; De Wael, K.; Janssens, K. Photodegradation Mechanisms and Kinetics of Eosin-Y in Oxic and Anoxic Conditions. *Dyes Pigments* **2017**, *145*, 376–384. https://doi.org/10.1016/j.dyepig.2017.06.031.

(32) Hughes, R. W.; Lott, M. E.; Bowman, J. I.; Sumerlin, B. S. Excitation Dependence in Photoiniferter Polymerization. *ACS Macro Lett.* **2023**, *12* (1), 14–19. https://doi.org/10.1021/acsmacrolett.2c00683.

(33) Wang, Y.; Meng, H.-M.; Song, G.; Li, Z.; Zhang, X.-B. Conjugated-Polymer-Based Nanomaterials for Photothermal Therapy. *ACS Appl. Polym. Mater.* **2020**, *2*, 4258–4272. https://doi.org/10.1021/acsapm.0c00680.

(34) Sims, M. B.; Lessard, J. J.; Bai, L.; Sumerlin, B. S. Functional Diversification of Polymethacrylates by Dynamic β-Ketoester Modification. *Macromolecules* **2018**, *51* (16), 6380–6386. https://doi.org/10.1021/acs.macromol.8b01343.

(35) Lessard, J. J.; Scheutz, G. M.; Hughes, R. W.; Sumerlin, B. S. Polystyrene-Based Vitrimers: Inexpensive and Recyclable Thermosets. *ACS Appl. Polym. Mater.* **2020**, *2* (8), 3044–3048. https://doi.org/10.1021/acsapm.0c00523.

(36) Aruldass, S.; Mathivanan, V.; Mohamed, A. R.; Tye, C. T. Factors Affecting Hydrolysis of Polyvinyl Acetate to Polyvinyl Alcohol. *J. Environ. Chem. Eng.* **2019**, *7* (5), 103238. https://doi.org/10.1016/j.jece.2019.103238.